Schweizerische Meteorologische Anstalt
Institut suisse de météorologie
Istituto svizzero di meteorologia
Swiss Meteorological Institute

No. 177e

Climatology of atmospheric dispersion

Net radiation as a factor in atmospheric stability

Philippe Tercier, Payerne

June 1995

Arbeitsberichte der SMA
Rapports de travail de l'ISM
Rapporti di lavoro dell'ISM
Working Reports of the SMI

English translation of the original French version provided by the Translation Services of the European Commission in Brussels.

© SMA, Publikationen, CH-8044 Zürich

Schweizerische Meteorologische Anstalt
Krähbühlstrasse 58, Postfach
CH-8044 Zürich

Tel. (01) 256 91 11, Fax (01) 256 92 78, Telex 81 73 73 met ch

Climatology of atmospheric dispersion

Net radiation as a factor in atmospheric stability

Philippe Tercier

June 1995

Atmospheric stability 551.501.721
Radiation 551.521

Summary

Any study of the dispersion of pollutants released into the atmosphere close to the ground must take account of the state of stability of the atmosphere. This state of stability, or turbulence, is the result of the joint action of thermal and advective forces. The first methods used to calculate it, introduced by Pasquill (Pasquill and Smith 1983), Turner (1964) and the German TALuft guidelines (Henselder 1986) are based on synoptic observations. Polster (1969) made comparisons using net radiation and wind speed and suggests a new way of calculating stability. The aim of the present study is to devise a system applicable to Switzerland, using a Holtslag and Van Ulden (1983) method for determining net radiation and considering only parameters measured at stations belonging to the Swiss Meteorological Institute's ANETZ network. The adjustments have been made on the basis of two programmes currently in progress at Payerne for measuring (inter alia) net radiation and its components, and conventional measurements from an ANETZ station.

Résumé

Toute étude de la dispersion de polluants relâchés dans l'atmosphère proche du sol fait intervenir les conditions de stabilité de l'atmosphère. Cette stabilité, qui exprime également l'état de turbulence, résulte de la conjugaison des forces thermique et d'advection. Les premières méthodes pour la calculer, introduites respectivement par Pasquill (Pasquill et Smith, 1983), Turner (1964) ou encore les directives allemandes TALuft (Henselder, 1986), sont basées sur les observations synoptiques. Polster (1969) a fait des comparaisons en utilisant le bilan du rayonnement et la vitesse du vent et propose un schéma de calcul de la stabilité. Le but du présent travail est de reprendre une paramétrisation du bilan du rayonnement due à Holtslag et Van Ulden (1983) en ne faisant intervenir que des paramètres mesurés aux stations du réseau ANETZ de l'Institut Suisse de Météorologie afin de proposer un schéma adapté à la Suisse. Les ajustements ont été réalisés sur la base de deux programmes de mesures qui se déroulent à Payerne, comprenant entre autres le bilan du rayonnement et ses composantes ainsi que des mesures conventionnelles d'une station ANETZ.

Zusammenfassung

Bei der Bestimmung der Ausbreitung von Luftschadstoffen sind die Bedingungen der atmosphärischen Stabilität massgebend. Diese Stabilität, welche ebenso den Turbulenzzustand andeutet, resultiert aus der Zusammenwirkung der thermischen und der advektiven Kräfte. Die ersten zu ihrer Bestimmung entwickelten Methoden von Pasquill (Pasquill und Smith, 1983), von Turner (1964) und den deutschen Richtlinien TALuft (Henselder, 1986) stützen auf synoptischen Daten. Polster (1969) hat Vergleiche unternommen, wobei er die Strahlungsbilanz und die Windgeschwindigkeit eingesetzt hat, und daraus ein neues Schema erarbeitet. Die vorliegende Arbeit hat zum Ziel die zur Berechnung der Strahlungsbilanz von Holtslag und Van Ulden (1983) vorgegebene Parametrisierung zu übernehmen und sie für den ANETZ-Datensatz der Schweizerischen Meteorologischen Anstalt (SMA) anwendbar zu machen, um dann ein für die Schweiz angepasstes Schema vorzuschlagen. Die Anpassungen erfolgen aufgrund von zwei Messprogramme, die zurzeit in Payerne durchgeführt werden, wo u.a. die Strahlungsbilanz und ihre verschiedenen Komponenten sowie die wichtigsten konventionellen Grössen einer ANETZ-Station erhoben werden.

Riassunto

Tutti gli studi sulla dispersione degli inquinanti atmosferici vicini al suolo fanno intervenire le condizioni di stabilità dell'atmosfera. Questa stabilità, che esprime d'altra parte anche lo stato di turbolenza, viene determinata dall'insieme delle forze termiche e d'avvezione. I primi metodi di calcolo di Pasquill (Pasquill e Smith, 1983), di Turner (1964) et delle direttive tedesche TALuft (Henselder, 1986), sono basati sulle osservazioni sinottiche. Polster (1969) ha applicato dei metodi comparativi utilizzando il bilancio della radiazione e la velocità del vento e ha proposto uno schema di calcolo della stabilità. Lo scopo del presente lavoro é di riprendere un metodo di Holtslag e Van Ulden (1983), per determinare il bilancio della radiazione e di fare intervenire solamente i parametri misurati dalle stazioni della rete ANETZ dell'Istituto Svizzero di Meteorologia al fine di proporre uno schema adattato alla Svizzera. Gli adattamenti sono stati realizzati sulla base di due programmi di misura che si svolgono a Payerne e che comprendono, fra l'altro, il bilancio della radiazione e le sue componenti, come pure le misure convenzionali di una stazione ANETZ.

Abbreviations

ANETZ	Automatic Network (network of automatic stations operated by the SMI)
BSRN	The "Baseline Surface Radiation Network" project
COMRAD	Project for comparing radiometers
ENET	"ErgänzungsNETz": a network complementary to ANETZ
ENV	Environmental Meteorological Department
IEA	International Energy Agency
MET	Middle European Time
OFEFP	Federal Department of the Environment, Forestry and the Landscape
SMI	Swiss Meteorological Institute (French : ISM)
TALuft	Technical Guidelines on Clean Air (Germany
UT	Universal Time
WMO	World Meteorological Organization

Table of Contents

1. INTRODUCTION

Swiss legislation on environmental protection requires that all plant construction or modification plans be subject to an environmental impact assessment, particularly where polluting emissions are released into the atmosphere. The thermodynamic state (or degree of stability) of the atmosphere close to the ground, coupled with advection, determines the atmosphere's ability to disperse local or regional pollution. This atmospheric dispersion capability is calculated using mathematical models for which numerical or statistical good quality data on the layer of atmosphere concerned are required.

The methods (also known as "schemes") used for calculating atmospheric stability are those put forward by Pasquill (Pasquill and Smith, 1983), Turner (1964), the German TALuft guidelines (Henselder, 1986) and Polster (1969). The first two of these schemes use synoptic data, particularly cloud cover, observation of which is indeed still carried out at most ANETZ stations but often with insufficient frequency for this particular application. Only a few stations observe the cloud cover eight times a day - which would be sufficient for these purposes. The rest provide observations only three times a day and none at night. Furthermore, the topography of Switzerland is such that it would be difficult to use these observations as the basis for interpolating spatio-temporal cloud cover figures. The estimation of cloud amounts has therefore been dealt with in a separate chapter. The Vogt-Polster scheme is the result of a study correlating "synoptic" parameters with more direct measurements of air stability such as the vertical temperature gradient (measured at intervals of 100m) or net radiation. In Switzerland, these two parameters are seldom measured. The new national network for monitoring air quality (NABEL), consisting of 16 stations, includes a measurement of net radiation.

To meet the pressing demand for a gaussian-type model of atmospheric dispersion for use in impact studies, hourly series of stability figures were initially produced from simple but statistically acceptable estimates of net radiation based on ANETZ data. It proved necessary to adapt the Pasquill-Turner and TALuft schemes separately. This procedure is set out in Annex 1. The first "Dispersion climatology" log-books, drawn up separately for each ANETZ station, were prepared using this provisional method.

The purpose of this study is to bring the definitions which have been used for the last few decades into line with the new measurements which have been introduced into the ANETZ network, with a view to producing time sequences of stability figures. The reference scheme is Polster's, and the entry data include net radiation as well as wind speed. A method developed by Holtslag enables net radiation to be calculated on the basis of conventional climatological measurements. The ANETZ network has the advantage of measuring global radiation, and thus provides more accurate figures than would be obtained by calculating the global radiation on the basis of the sun's elevation and the cloud cover. The adjustments to this method have been made on the basis of two programmes currently in progress at Payerne for measuring (inter alia) net radiation and its components, as well as conventional measurements from an ANETZ station. A comparison of the measurements obtained by these two programmes, which overlap to some extent but use equipment of different design, has shown how tricky it can be to measure net radiation and its components. Moreover, these observations have, more than once, raised question marks over some of the adjustments made during the initial phase of this study.

The report is structured as follows. Chapter 2 provides a survey of the types of measurement involved. The problem of estimating cloud cover (chapter 3) logically precedes the parametrization of net radiation and its components (chapter 4). The statistical analysis of the data was carried out using S- PLUS software (Statsci, 1991).

2. MEASUREMENTS

The hourly data used in this study come from the ANETZ station at Payerne, the COMRAD project (comparison of radiometers) and to a lesser extent the COMVENT project (comparison of anemometers) begun at Payerne in late 1987. The measurement period chosen was three years - from December 1987 to November 1990. Apart from the usual climatological and synoptic measurements, THE ANETZ network provides figures for global radiation and the temperature at 5cm above the ground. These data are recorded at MET in the department's TIDOMES data bank, in which the COMRAD hourly average figure is recorded 40 minutes before the ANETZ average.

2.1 The COMRAD project

The aim of the COMRAD project (Wasserfallen, 1991) was to compare the technical performance of different radiometers and sunshine recorders. From 1988 to 1993, the project measured the principal components of solar radiation and a number of conventional parameters. The radiation parameters were given different names by different authors, and the nomenclature also depended on whether it related to ground level radiation or to a layer of the upper atmosphere:

Global solar radiation	(pyranometer)	G	=	$K\downarrow + K\downarrow dif$
Reflected global solar radiation	(pyranometer)	R	÷	$K\uparrow$
Diffuse solar radiation	(pyranometer)	D	÷	$K\downarrow dif$
Downward total radiation	(pyrradiometer)	$Q\downarrow$	=	W + G
Upward total radiation	(pyrradiometer)	$Q\uparrow$	=	E + R
Net radiation	(differential pyrradiometer)	Q^*	=	(G-R) + (W-E)

and the calculated components of long-wave radiation near the ground:

Atmospheric radiation	W	÷	$L\downarrow$
Terrestrial radiation	E	÷	$L\uparrow$

Thus the main balances - for shortwave radiation K^*, longwave radiation L^* and net radiation Q^* can be calculated. The net radiation figure is thus obtained in two ways: by direct measurement and by measuring its components. The symbols for these balances are marked with an asterisk: unmarked letters are reserved for other values. In the case of sunshine duration the measurement method adopted is as follows:

Sunshine duration	(sunshine recorder)	S	in 1/100 hours

2.1.1 Measurement problems

As long ago as September 1992, measurements taken at Payerne under the BSRN (Baseline Surface Radiation Network) project run by the World Meteorological Organization (WMO, 1991) brought to light a number of discrepancies in the values for longwave radiation calculated on the basis of pyrradiometer readings and measured by Funk-type balance meters. This problem is discussed in the WMO guidelines (WMO, 1990). It particularly affects the determination of daytime longwave radiation when the solar radiation is intense. Comparisons with readings from pyrgeometers have shown that the calibration coefficients of pyrradiometers, which are not protected from direct sunlight, consistently show errors when the radiation is intense. The error may be as much as 5% in the case of terrestrial radiation (E), and may result in an underestimation of the value of Q^*. This anomaly does not appear in the figures for atmospheric radiation when based on measurements of diffuse radiation ($W=Q\downarrow dif - K\downarrow dif$) since the measuring instruments are protected from direct sunlight. For these three values (E, W, Q^*), comparison of the results obtained using pyrradiometers and pyrgeometers over a 12-month period (September 1992 to

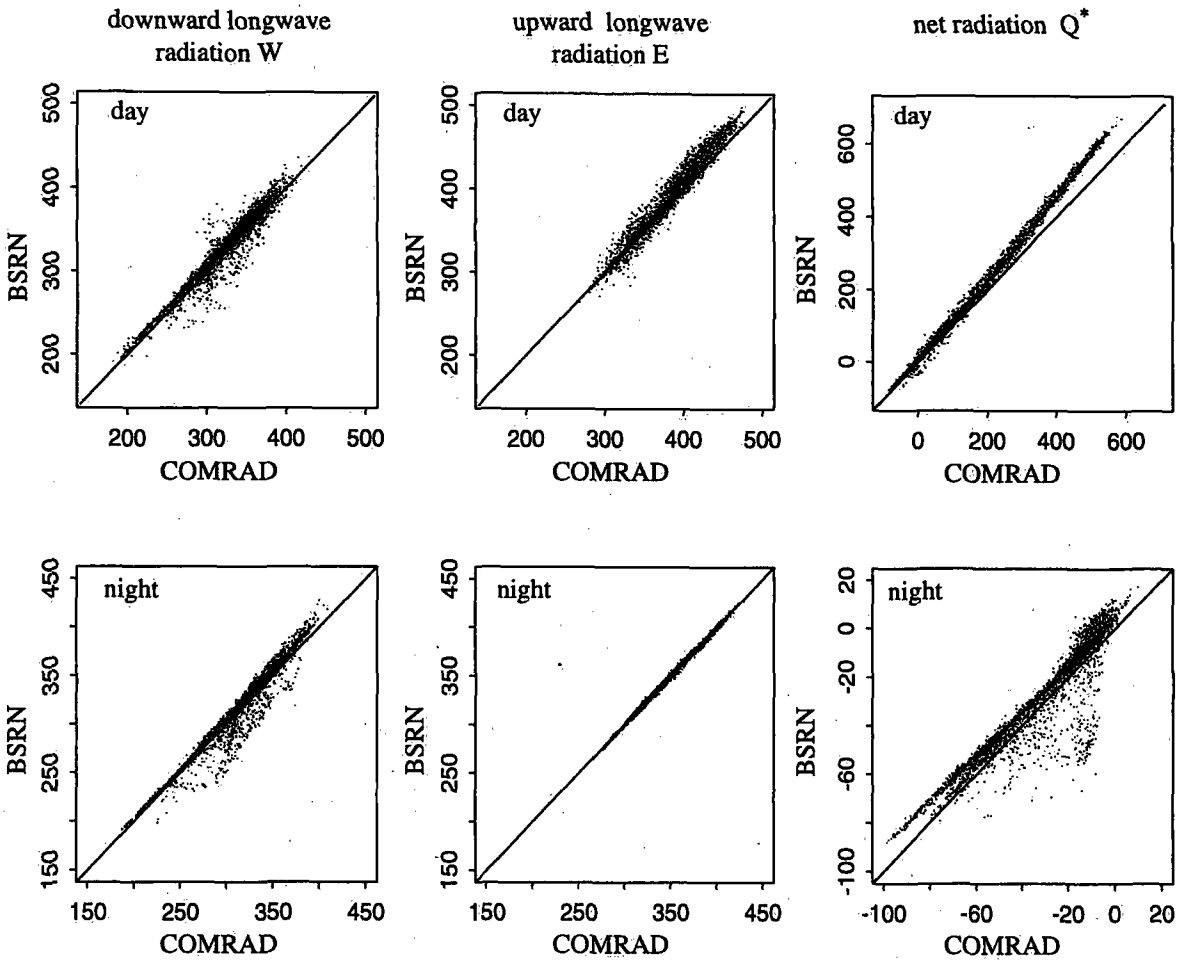

Figure 1. Comparison of the values (in W/m^2) for atmospheric, terrestrial and net radiation as between the COMRAD and BSRN projects, September 1992 to August 1993.

August 1993) enables us to suggest a number of corrections to measurements made under the COMRAD project.

As shown in Figure 1, the pyrradiometers (pd) used in the COMRAD project undervalue the parameters indicated. These discrepancies appear at night as well as during the day. In the case of **atmospheric radiation** (W), there is a virtually constant difference of less than 2%.

$$W_{corrected} = 1.0175 W_{pd} \quad (1)$$

This correction is valid for both day and night readings. Some discrepancies occurring towards the end of the night, and which correspond to a considerable overvaluation of the COMRAD figure, are due mainly to dew or frost forming on the pyrradiometer dish. This results in negative balance values which are too low, as can be seen from the spread of dots in Figure 1 (right hand graph).

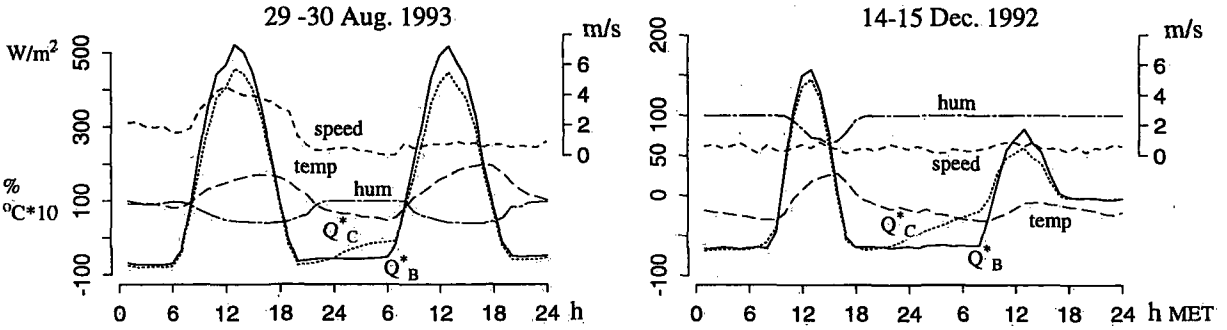

Figure 2. Summer and winter episodes in the measurement of net radiation by COMRAD Q^*_C and BSRN Q^*_B

Figure 2 illustrates the effects of summer dew and winter frost. Insufficiently ventilated instruments are affected by these phenomena, which occur under certain thermodynamic conditions determined by the relative humidity, temperature and wind speed. Roughly 6% of instrument errors (> 20 W/m^2) are associated with this type of phenomenon.

The figures for nocturnal **terrestrial radiation** (E) are in complete agreement, but the daytime figures must be corrected to allow for the intensity of direct sunlight.

$$E_{corrected} = E_{pd} + 0.0164G + 0.000015E_{pd}G \qquad (2)$$

An alternative correction, $E_{corrigé} = E_{pd} + 0.023G$, is simpler and is acceptable: however, under conditions of strong sunlight it becomes less accurate.

A similar correction is required for the daytime **net radiation** Q^* :

$$Q^*_{corrected} = 0.914Q^*_{pd} + 0.1G + 0.0000816Q^*_{pd}G \qquad (3)$$

At night, the COMRAD measurements overvalue the radiation loss (Abstrahlung), especially at values below -20 W/m^2. The COMRAD figures are ambiguous at the lower end of the range: some closely match the BSRN measurements while others (the majority) differ significantly from them. The optimal correction for the figures as a whole is 2 +0.95Q^*, but to concentrate on the discrepancy in the majority of readings would require a correction of 4 +0.95Q^*. The regression between the difference $W_{corrected}$-E and Q^* in the COMRAD figures confirms the correction 4 +0.95Q^*. As already stated, the (dispersed) discrepancies corresponding to COMRAD figures which are much too low are due to temporary factors such as dew and frost. These changes in the figure for nocturnal net radiation are responsible for a residual error of less than 7 W/m^2.

Subsequently, the "corrected" COMRAD figures for the period 1988-90 will have been corrected by equations (1) to (3) and by 4 +0.95Q^* for the nocturnal net radiation figures. Finally it should be noted that these corrections relate only to the COMRAD project's pyrradiometers and are not applicable to other instruments.

2.2 The ANETZ, ENET and NABEL networks

Hächler (1993) gives information on the SMI's observation and measurement networks. The ANETZ network consists of more than 70 stations throughout Switzerland. Since 1978 it has steadily been replacing conventional weather stations. A complete list of the stations together with their geographical coordinates (useful for the calculation proposed in Annex 3), distances and certain details relevant to this study are given in Annex 5. At each station, between 15 and 25 meteorological parameters are measured automatically every 10 minutes. Some visual observations are still carried out, but not according to a schedule common to all stations. The ENET network is chiefly concerned with wind measurements. Few of its stations take a broader range of measurements of direct use for the purposes of this study. They may, however, be useful in combination with ANETZ stations.

From 1989 to 1991, the OFEFP completely reorganized the NABEL network (national network for observing air pollution). Filliger (1993) has given a complete description of the reorganization. Under the new system, each station carries out a series of measurements including net radiation and wind speed - which are the two data needed to determine atmospheric stability (see Annex 1).

The locations of the ANETZ, ENET and NABEL stations are indicated on the same map in Annex 5.

3. ESTIMATING THE CLOUD COVER

Not all ANETZ stations have the same programme for cloud observation. Fourteen stations located in open country (including Payerne) or in valleys measure cloud amounts every three hours. Thus hourly figures for cloud cover can be produced by assigning the observed value to the hour preceding and the hour following the observation. The other stations make three observations - at 06.00, 12.00 and 18.00 hours UT. It is therefore a matter of deciding which parameters measured by the ANETZ network express sufficiently clearly the ground-level effects of cloud cover by day and at night, so that hourly figures can be produced.

Figure 4 (top) on page 8 shows the daily and yearly distribution of the frequency of observed cloud cover (expressed in decimals). Without going into details it is clear that "clear sky" (0:8, i.e. N=0) observations are much more frequent at night than during the day, and that completely overcast skies (8:8, i.e. N=1) tend to be recorded at night rather than smaller cloud amounts (7:8 to 5:8). This is at least partly due to the fact that it is more difficult to make precise observations of cloud cover at night. Nevertheless, daily variations in cloud amounts occur chiefly when there is low to medium cloud cover, regardless of the time of year (e.g. regardless of the convective conditions which obtain in Summer). The value N>1 indicates fog.

3.1 The Albisser method, sunshine duration and global radiation

A method for estimating total cloud cover at **night** was developed by Albisser (1983). This method takes account of the difference in temperature between 2m and 5cm above ground level, precipitation, relative humidity and wind speed. Details of the algorithm are given in Annex 2, together with a variant of the class limits for temperature differences - the purpose of which is to achieve a more even balance between the estimated occurrences of zero or moderate cloud cover and the number of occurrences actually observed. Figure 3a shows how the results of this method correlate with observations. The dotted curve omits the early and late night, when the method works less well.

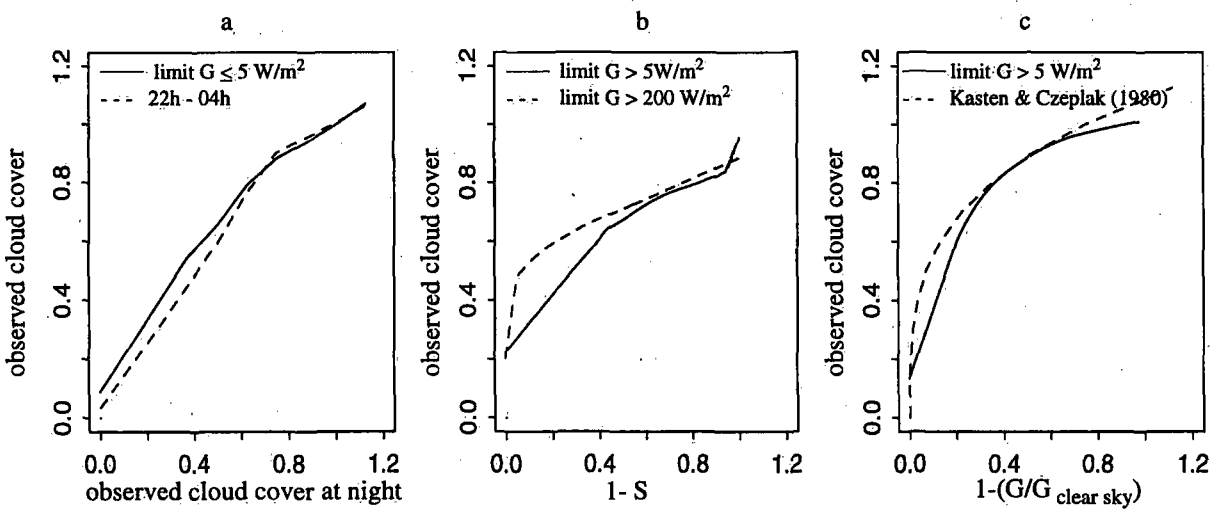

Figure 3. Correspondence between observed cloud cover and simulated cloud cover, Payerne 1988-1990, as calculated: (a) by the modified Albisser method; (b) by the sunshine duration; and (c) by the global radiation G

Daytime figures for sunshine duration S and global radiation G are affected by passing clouds. Nevertheless, these figures reflect responses which differ physically not only from one another but more especially from the visual observation of cloud cover. When there is little observed

(i.e. actual) cloud cover, the spatial distribution of the clouds can make a tremendous difference. At midday, for example, an area of clear sky or cloud on the horizon will not be registered by the automatic measurement system, whereas a human observer will take account of them. Allowance must also be made for the extent to which the sensitivity threshold of sunshine recorders (solar irradiance >120W/m^2, ANETZ: >200W/m^2) affects the figures for sunshine duration (Heimo, 1990). The dotted curve in Figure 3b shows how the figures are altered by omitting the beginning and the end of the day. Statistically, therefore, sunshine duration has insufficient discrimination under slightly or very cloudy conditions (see Figure 3b, curve cut-off points). It has, however, the advantage of being virtually unaffected by seasonal variation. Global radiation (Figure 3c) also performs poorly when cloud cover is slight. It is affected by the density and thickness of the clouds and is thus a better indicator of very cloudy conditions. Tests have been carried out on a number of ways of compensating for these discrepancies between measurement and observation. The unbroken curve in Figure 3b may be expressed by the following polynomial:

$$\text{Cloud cover} = 0.22 + 1.04\,x - 0.33\,x^2 \qquad \text{where } x = 1 - S, \quad S \text{ given in hours/100} \qquad (4)$$

or by moderating the greater indeterminacy around sunrise and sunset and when there is full sunshine but the sky is not completely clear:

$$\text{Cloud cover} = 0.92\,x^{0.5} + 0.08\,x^2 \qquad (5)$$

The unbroken curve in Figure 3c is well expressed by the following polynomial:

$$\text{Cloud cover} = 0.16 + 1.41\,x + 1.22\,x^2 - 3.88\,x^3 + 2.16\,x^4 \qquad \text{where } x = (1 - G/G_0), \qquad (6)$$

or as above in order to take better account of the greater indeterminacy around sunrise and sunset and when there is full sunshine:

$$\text{Cloud cover} = 0.79\,x^{0.5} + 0.80\,x - 0.59\,x^2 \qquad (7)$$

G_0 is the global radiation when the sky is clear (cloudless), and its evaluation is dealt with in paragraph 4.2 and in Annex 3. When $G>G_0$, the inverse value of the ratio is used; this represents a random redistribution of uncertain instances (at the measurement limits) at sunrise and sunset, and of cases where the sky is not completely clear or not completely overcast but the cloud reverberation is particularly intense.

The dotted curve in Figure 3c corresponds to equation 8 (Kasten and Czeplac, 1980):

$$1 - \frac{G}{G_0} = -b_1 N^{b_2} \qquad \text{where} \quad b_1 = -0.75 \quad \text{and} \quad b_2 = 3.4 \qquad (8)$$

This type of equation accentuates the indeterminacy where cloud cover is slight. Bosshard (1992) has established the b1 and b2 parameters for the different types of cirrus, altocumulus, stratus and cumulus cloud as observed at several ANETZ stations. His study shows that, given equal total cloud cover, global radiation is most attenuated by stratus cloud. Altocumulus and cumulus produce virtually the same degree of attenuation, while cirrus has only a slight screening effect.

Occurrences of fog, by night and by day, are determined using an Albisser criterion which requires that there be no precipitation, that the air temperature at 2m AGL be no higher than at 5cm AGL, the relative humidity greater than 94.5% and the wind speed less than 1.2 m/s.

Observed cloud cover is expressed in discrete values. To compare the procedures, the values of $1 - S$ or $1 - G/G_0$ can also be made discrete. To show as clearly as possible the distribution of the observations, the following classes (Table 1) have been calculated in accordance with the inverse application of equations 4 to 7.

Table 1. Class limits for the distribution of the values of 1-S or 1 - G/G_0 in relation to the distribution of observed cloud cover.

0 1 2 3 4 5 6 7 8	observed cloud cover
] 0.02], 0.13, 0.28, 0.37, 0.46, 0.55, 0.65, 0.99, 1.01	for equation No.4
] 0.02], 0.16, 0.33, 0.44, 0.55, 0.66, 0.76, 0.99, 1.01	for equation No.5
] 0.02], 0.14, 0.27, 0.39, 0.51, 0.63, 0.76, 0.88, 1.01	for equation No.6
] 0.11], 0.24, 0.34, 0.46, 0.55, 0.63, 0.77, 0.92, 1.01	for equation No.7

The coefficients used for correlating calculated and observed cloud amounts during the three year measurement period are given in Table 2. The day-night limit is set by the value of 5 W/m^2 for the global radiation measured. The algorithms of the methods used and the conditions applied in estimating the cloud cover are set out in Annex 2. The Albisser (1993) method is applied only at night.

Table 2. Coefficients for correlating observed cloud amounts with those calculated by various methods

estimated cloud cover / method	A hourly substitution parameters	idem A + observed cloud cover at 6, 12 and 18 hrs *	B substitution param. averaged over 3 consecutive hours	idem B + observed cloud cover at 6, 12 and 18 hrs *
Albisser (modified)	0.79 (0.81)	(0.85)	----	----
Sunshine duration	0.77	0.89	0,80	0.89
Equation No.5	0.78	0.89	0.80**	0.91**
Ratio $G/G_{clear\ sky}$	0.74	0.82	0.77	0.83
Equation No.7	0.75	0.89	0.77	0.91
* including extrapolation ± 1 hour ** equation 5 with coefficients in the order 0.88 and 0.12				

The above methods are all difficult to apply at sunrise and sunset. If these difficult periods are discounted, the coefficients improve by 5% at most. A practical improvement may be achieved by reintroducing into the series the figures for observed cloud cover, since this observation is carried out at most weather stations at least three times a day - at 6, 12 and 18 hours UT. The Albisser (1983) method takes account of the 6 and 18 figures only. By extrapolation, moreover, the observed cloud amount may be assumed to hold good one hour before and one hour after the time of the observation. The coefficients given in columns 2 and 4 of Table 2 simply serve to show the maximum degree of correlation possible under the procedure.

Given the nature of the sunshine duration measurement, a closer statistical correspondence with the cloud cover actually observed at specific times would probably be achieved by taking the average figure for sunshine duration over three consecutive hours. Comparison of the correlations between columns 1 and 3 and columns 2 and 4 in Table 2 shows only a slight improvement. Nevertheless, this option brings the distribution of figures for slight cloud cover (Figure 4b) considerably more into line with that of the figures for observed cloud cover. There is no such improvement in the case of global radiation (average calculated on the G/G_0 ratio, Figure 4d).

3.2 Summary of the options

In accordance with the measurements and observations carried out at the SMI's weather and climatology stations, the following options are available for producing hourly figures for net radiation Q^* parametrized with, among other things, total cloud cover N.

The SMI's first "Dispersion climatology" log-books use the following simple algorithms, in which the effect of cloud cover is implicit in G and ΔT:

daytime ($G>5$ W/m^2) : $Q^* = -13.06 + 0.60\,G$ values for Q^* not corrected.

night-time ($G \leq 5$ W/m^2) : $Q^* + \Delta T$ = temperature difference between 2m and 5cm

Where cloud cover is observed every three hours, the hourly sequence can be obtained by assigning the observed value to the hour before and the hour after the time of observation. Otherwise the options set out in the previous paragraph can be adopted, depending on which of the two measurements one has available. One can then go on to calculate the net radiation as follows:

- for daytime ($G>5$ W/m^2), use the sunshine duration averaged over three consecutive hours S_3 , and the equation:

$$\text{cloud cover} = 0.88\,x^{0.5} + 0.12\,x^2 \qquad \text{where } x = 1 - S_3$$

If these values need to be changed into discrete values, use the following classes:

] 0.02], 0.16, 0.33, 0.44, 0.55, 0.66, 0.76, 0.99, 1.01

- for night-time ($G \leq 5$ W/m^2), use the modified Albisser algorithm (see Annex 2).

Furthermore, where cloud cover is observed three times a day (as is the case at most ANETZ stations), these data are introduced and extrapolated one hour before and after the observation time: N(6h±1, 12h±1, 18h±1).

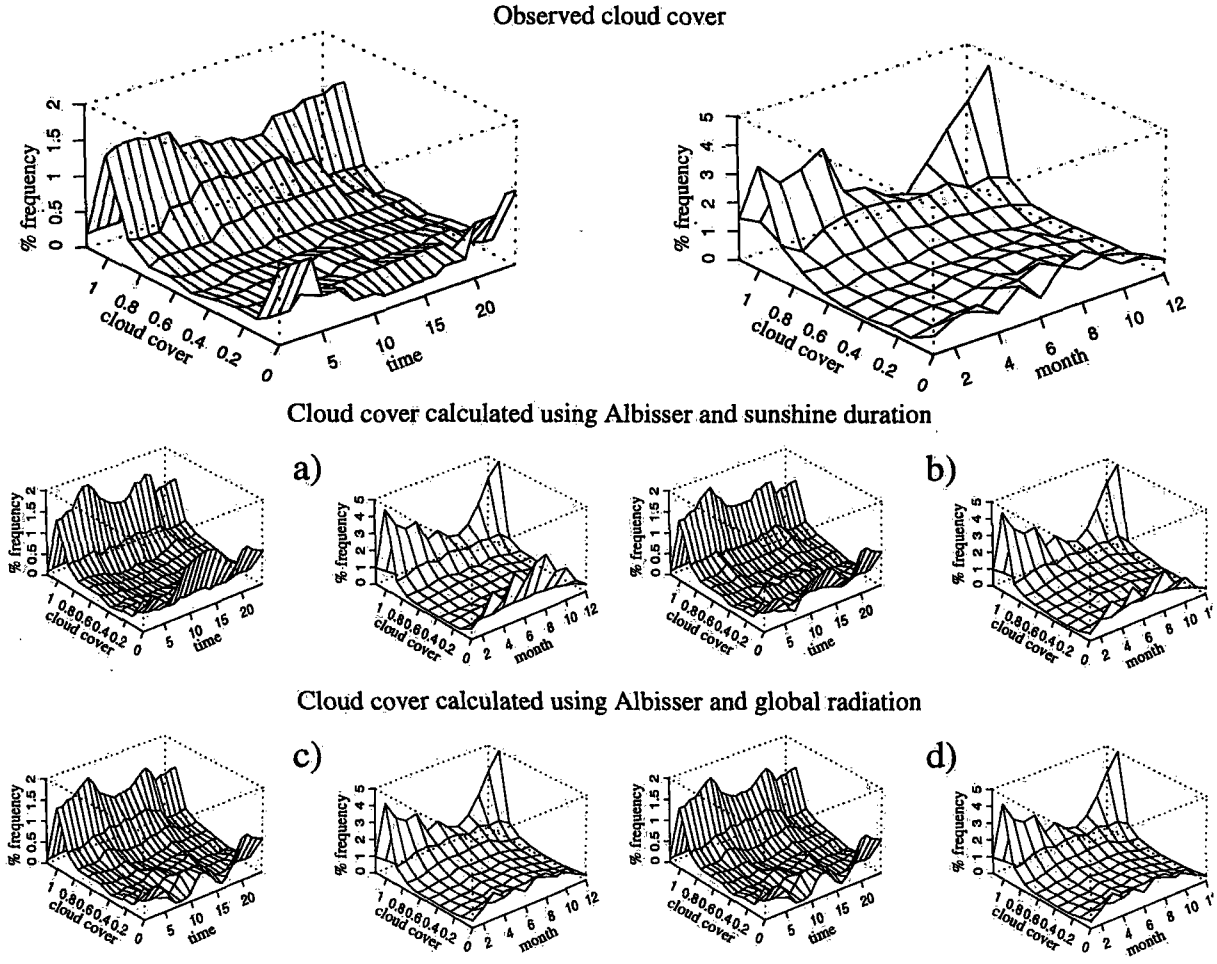

Figure 4. Daily and annual variations in the observed or calculated cloud cover, Payerne, 1988-1990
(a to d: calculated cloud cover only, i.e. without introducing the observations made at 6, 12 and 18 hrs)
(a) and (c): sunshine duration/hourly global radiation
(b) and (d): sunshine duration/global radiation averaged over 3 hours

4. NET RADIATION

The ground-level net radiation Q^* can be estimated by parametrizing the terms of the following equation:

$$Q^* = (1 - r)\,G + W - E \qquad (9)$$

where r is the albedo at ground level. Terms W and E are parametrized in accordance with the proposals made by Holtslag (1983).

4.1 Albedo

In principle, ANETZ stations take their measurements on a regularly-mown grassy surface, as is the case at Payerne. Global radiation G is measured at all these stations. The albedo is determined using the equation $R = rG$. Its average value (COMRAD measurements limited to $G > 5$ W/m^2) is 0.24, with a variation of 0.02 if the occasional values greater than 0.4 seen in Figure 5a are disregarded. (The annual averages were 0.255 in 1988, 0.244 in 1989 and 0.236 in 1990). Average albedo decreases slightly where global radiation increases: $\bar{r}(G>300\ \text{W/m}^2) = 0.23$. Figure 5a clearly shows that the measurements become less accurate where global radiation falls below 300 W/m^2. This is partly due to the ground conditions and the sensitivity of the radiation detectors. The dots which lie outside the dense distribution generally denote snow on the ground.

To homogenize equation 9 as far as possible, it is useful to know the stability of the value of r calculated on the basis of the four factors measured (corrected values). It varies with global radiation to a greater extent than the variation indicated above. Regression gives $r = 0.24 - 0.00006G$, and this correction will be taken into account when calculating Q^*.

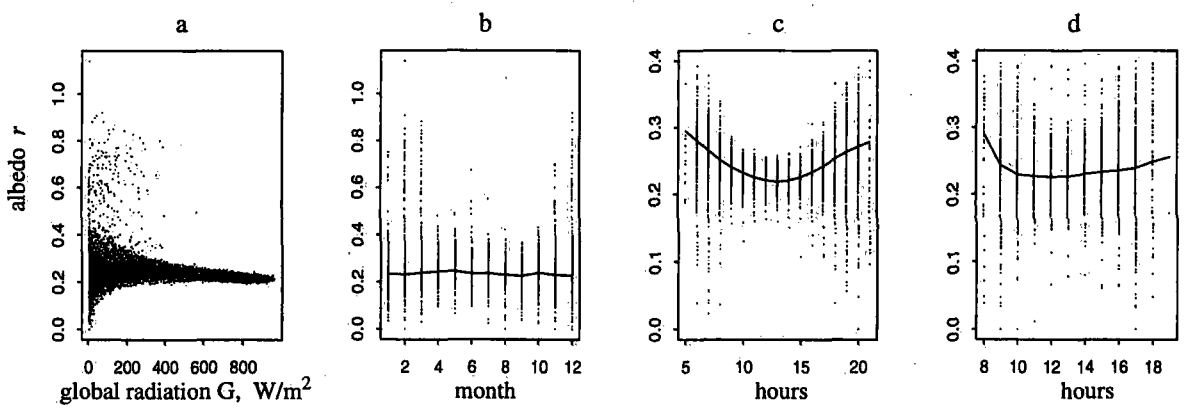

Figure 5. Albedo measurements from December 1987 to November 1990/
a) as a function of global radiation G
b) annual variation
c) daily variation, April to September
d) daily variation, October to March

The average monthly albedo (Figure 5b) does not vary in the course of a year, but the values are more dispersed in Winter owing, in part, to the snow cover. Only the albedo values lower than 0.4 have been used to test the daily variation. Discounting the first and last hour of daylight (for which there are few values), a variation in the average albedo clearly appears in Summer (see Figure 5c) but is negligible in Winter (Figure 5d). Nevertheless, there is a marked variation all year round if account is taken only of very sunny days or periods - as can be seen from Figures 6a and 6c. The dotted line in both these Figures indicates the lack of variation in albedo under overcast conditions. Some of these variations are certainly due to instrument problems. The type of ground surface may also introduce a slight non-linearity between incident and

reflected solar radiation. The equation $r = \frac{R/\bar{R}}{G/\bar{G}}(\bar{R}/\bar{G})$ shows that the way in which albedo r varies in Figure 6 depends on the ways in which the average values relate to the whole. Thus the concave shape implies $R/\bar{R} > G/\bar{G}$. For the month of July in the three years during which measurements were taken, $\bar{R} = 145$ W/m^2 and $\bar{G} = 632$ W/m^2, and the ratio $\bar{R}/\bar{G}$ is 0.23. For the months of December and January in the three years of measurements, $\bar{R} = 79$ W/m^2 and $\bar{G} =$ 276, and the ratio is 0.29. Figures 6b and 6d show how the ratios of R and G to their average figures behave. Since this variation occurs both in Summer and in Winter, it is unlikely to be caused by the type of ground surface and its effect on reflected radiation. Where instruments are concerned, the most serious relative measurement error might well arise from trying to capture the diffuse radiation (as part of the global radiation measurement G) when the sun is low on the horizon. This would produce the inequality $R/\bar{R} > G/\bar{G}$.

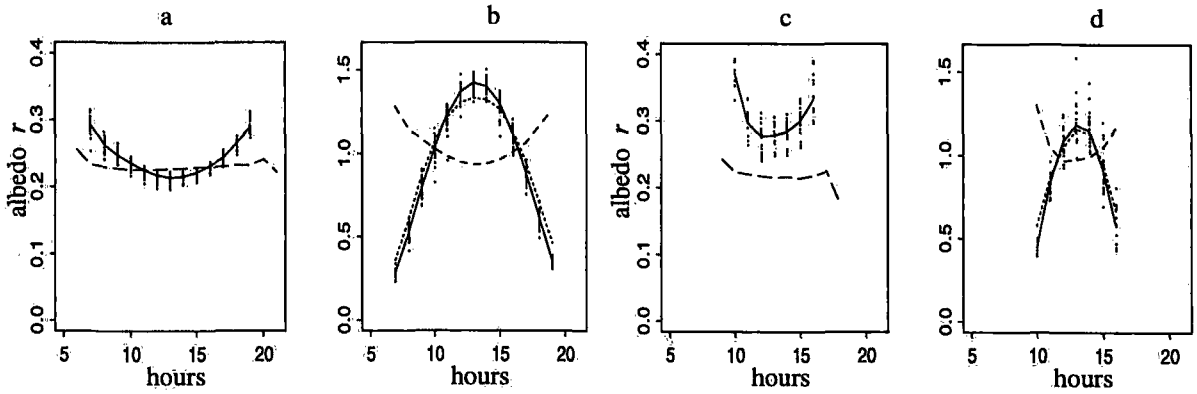

Figure 6. Daily variations in albedo and its components where sunshine duration exceeds 0.98/hour
a) July 1988-1990: albedo (- - -) where sunshine duration < 0.1
b) July 1988-1990: ratios $R/\bar{R}$ (.....), $G/\bar{G}$ (——) and $R/\bar{R} : G/\bar{G}$ (----)
c) December and January 1987-1990: albedo (- - -) where sunshine duration < 0.1
d) December and January 1987-1990: ratios $R/\bar{R}$ (.....), $G/\bar{G}$ (——) and $R/\bar{R} : G/\bar{G}$ (----)

The following equations might be used to take account not only of the slight variation in albedo caused by intense global radiation (as described earlier in this paragraph) but also of the variation which occurs under moderately to very clear skies in the morning and evening:

$$r = 0.24 \quad \text{where} \quad S < 0.3 \qquad \text{and} \qquad r = 0.3 - 0.00015\,G \quad \text{where} \quad S \geq 0.3 \qquad (10)$$

The very low limit required for sunshine duration S is partly due to the sensitivity threshold for this measurement.

4.2 Global radiation

Global radiation G is measured at all ANETZ stations. At present, Switzerland does not really have any spatial interpolation method for producing hourly radiation figures. Thanks to the work commissioned by the International Energy Agency (Zelenka et al., 1992), and for which the ANETZ network was one of the test bases, it has been possible to work out a series of daily - rather than hourly - figures for any location in Switzerland. Although measurements taken by satellite have been shown to complement these figures (d'Agostino and Zelenka, 1992), we are as yet unable to apply these methods on an hourly basis.

There are, moreover, quite a number of models for calculating global radiation G by first determining the amount of solar radiation under clear sky conditions G_o and then applying to this

figure the attenuation due to cloud cover N (Davies et al, 1988). In the previous chapter we referred to the Kasten and Czeplac model (1980). One simple parametrization of G_o is

$$G_o = a_1 \sin\phi + a_2 \quad (11)$$

where ϕ is the elevation of the sun. An algorithm for calculating the elevation of the sun, simplified but sufficiently precise for this application, is given in Annex 3. Values a_1 and a_2 are site-specific empirical coefficients which vary according to the regional average air turbulence under cloud-free (clear sky) conditions. They also depend on the quality of the equipment available for identifying those conditions.

Table 3. Calculating global radiation under clear sky conditions (equation No. 10)

Stations	Cloud cover	Sunshine duration	a1 (W/m2)	a2 (W/m2)	No. of instances	Residual error
Payerne COMRAD	≤ 1:8	-	1075	-79	1888	32
Payerne COMRAD	-	> 0.98	1077	-77	3047	29
Payerne ANETZ	≤ 1:8	-	1046	-82	1879	31
Payerne ANETZ	-	> 0.98	1046	-77	3024	30

Table 3 gives the coefficients a_1 and a_2 calculated for Payerne on the basis of the hourly sequences. It matters little whether interposed hourly figures are used or simply the 8 daily observations of cloud cover: the value of these coefficients is scarcely affected. The same cloud cover observation is used with the COMRAD and ANETZ measurements. Nor does it much matter whether "clear sky" is defined as cloud cover 0 or ≤1:8, since the values of a_1 and a_2 are hardly affected. The only difference is that the residual error increases slightly. The limit values $G > 5$ W/m^2 and $\phi > 5^\circ$ have been applied. At Payerne, the highest point on the horizon lies to the south-east and is no higher than 4.5° (Zelenka et al., 1991). At this level there is no discrepancy between the measured figure for global radiation and the figure derived from the visual observation of cloud cover, especially when the latter is slight.

Since the ANETZ network measures global radiation G, there is no point investigating any further the methods used for calculating this parameter.

4.3 Atmospheric radiation at ground level

Comparison of the measurements carried out under the BSRN and COMRAD projects (see paragraph 2.1.1) shows that the COMRAD figures for atmospheric radiation differ only slightly, but they do so systematically. They have been adjusted only for the sake of homogeneous data processing.

4.3.1 Clear weather

Under a clear sky (cloud cover < 3/8), atmospheric radiation W_o varies very little: the average daily variation is 30 W/m^2 in Summer, and practically nil in Winter. The annual variation increases from 260 W/m^2 (monthly average) in Winter to 340 W/m^2 at the height of Summer.

Figure 7 shows how the measured radiation W varies with the temperature at 2 metres above ground level (2m AGL) under clear weather conditions (W_o), distinguishing between daytime and night-time values. Figures 7a and 7c relate to an observed cloud cover of N=0. Clear sky conditions are designated, in Figure 7b, by a sunshine duration exceeding 0.98 and, in Figure 7d,

by a cloud cover of N=0 calculated in accordance with the Albisser (1983) method described in Annex 2 (unmodified version). The occurrences of fog (N=9) in Figure 7a correspond to maximum atmospheric radiation at a given temperature. The greater dispersion of night-time values also reflects the fact that cloud cover observation at night is less accurate than in daylight.

Atmospheric radiation under clear skies W_o may be parametrized using the absolute temperature T measured at 2m AGL in accordance with the Stefan-Boltzmann equation:

$$W_o = \varepsilon\sigma T^4 \ . \qquad (12)$$

where ε is the emissivity of the atmosphere and $\sigma = 5.67 \cdot 10^{-8}\ Wm^{-2}K^{-4}$, the Stefan-Boltzmann constant.

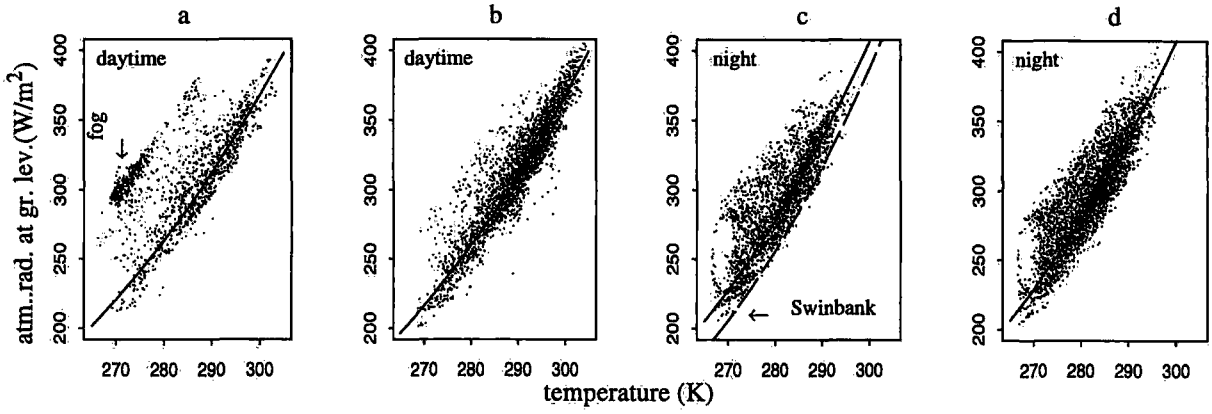

Figure 7. Atmospheric radiation W at ground level as a function of temperature (2m AGL) under clear skies by day and at night, Payerne, Dec.87 - Nov.90

a) by day, where observed cloud cover is N=0 or in fog where N=9
b) by day, where the measured sunshine duration exceeds 0.98
c) at night, with observed cloud cover N=0, (---) Swinbank curve $W_o = 5.31 \times 10^{-13} T^6$ (Holtslag)
d) at night, with cloud cover N=0 calculated using the original Albisser method

The regression curves in Figure 7 are drawn using the following equation and excluding the areas of major dispersion ("selection" column in Table 4).

$$\varepsilon = aT^b \qquad (13)$$

The characteristics of the curves are given in Table 4. The third and sixth lines refer to the cloud cover as calculated using the method described in paragraph 3.2 and the values corrected by equation No.1. The daytime curve is identical to the curve obtained using the observed cloud cover. The night-time curve gives a slightly (2%) lower value for ε at high temperatures.

Table 4. Relationship between emissivity ε and temperature (equation No. 12, Figure 7)

Reference	a	b	selection	total occurrences	select. occurr. (%)
Figure 7a	0.00346	0.957	$W < 1.64 \cdot 10^{-10} T^5$	1013	82
Figure 7b	0.00157	1.096	idem	3290	95
N(as per § 3.2)	0.00342	0.959	idem		
Figure 7c	0.00010	1.596	$W < 6.25 \cdot 10^{-13} T^6$	2660	77
Figure 7d	0.000136	1.542	idem	3928	81
N(as per §3.2)	0.000288	1.408	idem		

A number of authors have proposed empirical formulae for determining the emissivity ε of the atmosphere under clear sky conditions (Culf and Cash, 1993). Some have taken as their only parameter the atmospheric water vapour pressure at ground level e, but this means that emissivity is related to air temperature only in terms of water vapour pressure - which varies considerably from one locality to another. For emissivity to depend entirely on water vapour pressure, the atmosphere would have to be unchanging and homogenous. Reconsidering the question in the light of this objection, Swinbank (Holtslag and Van Ulden, 1983) has shown, by statistical correlation, that atmospheric radiation under clear sky conditions varies with T^6 (so that emissivity $\varepsilon \sim T^2$) and proposes the equation:

$$W_o = c_1 T^6 \qquad (14)$$

where $c_1 = 5.31 \cdot 10^{-13}$ $Wm^{-2}K^{-6}$, a value estimated to be on average accurate to within 5%. According to the measurements taken at Payerne in 1988-1990 and the interpolated hourly figures for observed cloud cover, $c_1 = 5.81 \cdot 10^{-13}$. If one takes only the figures for the cloud cover actually observed, and with a slightly better correlation (0.86 rather than 0.83), $c_1 = 5.65 \cdot 10^{-13}$, in which case - given an average temperature of 288K - the average emissivity ε is 0.826.

The Swinbank curve, which is intended to parametrize the occurrences of clear sky conditions both at night and by day, is given as a dotted line in Figure 7c. Since the measurements made at Payerne show that the two sets of figures - for night and daytime - do not really overlap, this equation is centred on neither of them. Idso and Jackson (1969) postulate that, just above and just below 273K, emissivity varies symmetrically. They propose equation No. 15:

$$\varepsilon = 1 - 0.261 \cdot \exp\left[-7.77 \times 10^{-4} \cdot (273 - T)^2\right] \qquad (15)$$

In Figure 8, the equations proposed by Swinbank (Holtslag and Van Ulden, 1983) and Idso and Jackson (1969) can be compared with the figures derived from the Payerne measurements. Comparison with the temperature measured at 30m AGL at Payerne confirms that, if the temperature at 2m AGL is used to determine W_o (little or no cloud cover), the day and night-time figures appear more closely related than the measured longwave atmospheric radiation would suggest. The fact is that if the temperature is measured at 30m AGL, where the direct ground effects are already much attenuated, the values for a and b in equation 13 are: By day a = 0.0083 and b = 0.80, at night a = 0.00394 and b = 0.941. These coefficients give values for which show a similar increase with temperature (see Fig. 8). If, on the other hand, the temperature is measured at 2m AGL, the daytime and night-time figures behave differently, and the difference is greater in Summer than in Winter. On a clear night in Summer the average temperature at 2m AGL is appreciably lower than that of the radiating atmosphere above that level. By day, on the other hand, it is only slightly higher. The average differences are considerably smaller in Winter.

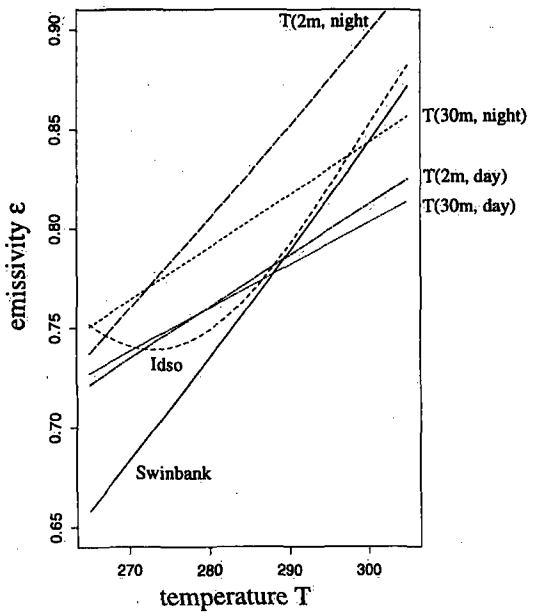

Figure 8. Emissivity ε of the atmosphere under clear sky conditions

In line with the approach adopted by Holtslag and Van Ulden (1983) for parametrizing terrestrial radiation on the basis of the measured temperature at 1m AGL, it is useful to analyse equation No.12 on the basis of the difference $T_{30m} - T_{2m}$. This equation can then be written as:

$$W_{o,\,30m} = W_{o,\,2m} + \Delta W\,(O\,(\Delta T)) = \varepsilon\,(\sigma T_{2m}^4 + 4\sigma T_{2m}^3\,(T_{30m} - T_{2m})) \qquad (16)$$

since the higher order values of ΔT are negligible. The measured values for ΔW in equation No.16 are given in Figure 9 as a function of net radiation. The graph on the left shows that, by day, this value is slightly negative; its absolute value scarcely exceeds 5 W/m^2, whatever the cloud cover and radiation intensity, because of the thermal mixing which occurs during the day. It follows that the daytime temperature at 2m AGL defines the state of the lower atmosphere fairly accurately and, on average, provides only a slight overestimation of its radiation.

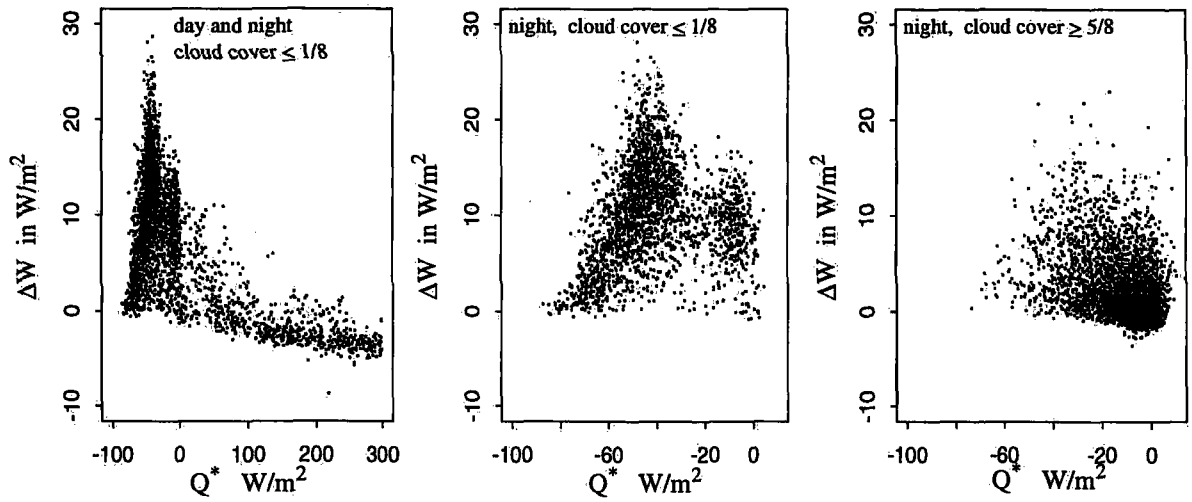

Figure 9. Distribution of the values of $\Delta W = 4\sigma T_{2m}^3\,(T_{30m} - T_{2m})$ as a function of net radiation

The graphs in the centre (observed cloud cover nil to very slight: N≤0.2) and on the right (considerable cloud cover: N>0.6) show the interrelatedness of $\Delta W(Q^*)$ at night. A comparison of the two graphs shows that ΔW is important only on clear nights. Furthermore, ΔW reaches its highest values when the relative humidity is less than 90%. Under these conditions there is intense stratification near ground level so that, if the temperature at 2m AGL is used (rather than some more representative temperature) in calculating atmospheric radiation, the result will be an even greater underestimation. The problem, then, is how to parametrize this correction. An attempt has been made in paragraph 4.3.3. In the central graph, the grouping of dots on the right hand side is due to the occurrence of dew or frost, as discussed in paragraph 2.1.1.

4.3.2 Cloudy weather

Atmospheric radiation at ground level increases with the cloud amounts N. Ground-level fog means maximum atmospheric radiation. Such circumstances are illustrated in Figure 7a. Paltridge and Platt (1976) propose the following linear equation:

$$W = W_0 + c_2 N \qquad (17)$$

where $c_2 = 60$ W/m^2 at temperate latitudes. This value corresponds to the maximum difference observable on the Q^* scale in Figure 9 between the groups of points on the graphs in the centre and on the right. In equation No.17, N ranges from 0 to 1.125 (N=9/8 in the case of fog). With the corresponding coefficients for determining W_0 (see Table 4), c_2 remains virtually constant (at an average value of 57) both by day and at night, and regardless of whether the cloud cover

is observed or is calculated using the method described in paragraph 3.2. The actual values obtained are as follows: c_2(by day, N_{obs})=57, c_2(at night, N_{obs})=56, c_2(by day, N_{cal})=58, c_2(at night, N_{cal})=56. The correlation between measured and calculated atmospheric radiation is as much as 0.86 (0.83 by day and 0.89 at night), with a residual error of less than 20 W/m^2 and a normal distribution of the residuals.

4.3.3 An alternative way of calculating nocturnal atmospheric radiation

For the purposes of calculating nocturnal atmospheric radiation, the temperature at 2m AGL yields the most accurate estimates when the lowest layer of the atmosphere is thermodynamically the most homogenous. This is probably the case when the wind (u) is moderate to strong, when there is precipitation and extensive cloud cover (N in 1/10) or when the humidity (h_{rel} in %) is high. When, on the other hand, these parameters have low values, the atmosphere close to ground level is more stratified, so that the temperature at 2m AGL becomes less representative. Thus equation No. 18 corresponds to equation No.17, with an additional term which, essentially, makes allowance for low values of the parameters N and u (the latter expressed in m/s). Since the sum $(N+\sqrt{u})$ ranges from 0.5 to 4 (10% of the values are between 0.5 and 1), the values of the exponential scarcely exceed 0.6. This term plays a less dominant role than in calculating terrestrial radiation (see equation No.22). The correction for humidity shows that it has an important influence on the measurement of temperature at 2m AGL. Since this influence is left out of account when determining W_0 (expressed as W/m^2), there is a close link between W_0 and h_{rel} .

$$W = 0.82W_0 + 48N + \dot{0}66h_{rel} + 11\exp[-(N+\sqrt{u})] \qquad (18)$$

The residual error here is, on average, 10% less than in the case of equation No.17. If the cloud cover is calculated using the method adopted in paragraph 3.2, this makes a considerable difference to the terms of equation No.18: their values are, in order, 0.84, 63, 0.35 and 57. This difference is partly due to the fact that the relative humidity and wind speed are already taken into account when calculating the cloud cover so as to distinguish occurrences of fog.

A large number of tests involving a great many conditional relationships between the parameters available at an ANETZ station have shown that the residual error can be reduced by, at most, 3 W/m^2. There is therefore no real reason for further complicating this parametrization.

4.4 Terrestrial radiation

Taking only the figures for clear weather, the monthly average terrestrial radiation measured at 2m AGL ranges from 320 W/m^2 in December-January to 400 W/m^2 in July. The average daily variation is greater than in the case of atmospheric radiation. It ranges from 110 W/m^2 in Summer to 60 W/m^2 in Winter.

Terrestrial radiation can be precisely calculated using the Stefan-Boltzmann equation, provided the ground radiation temperature is known. However, this temperature is hard to measure and figures are rarely available. ANETZ stations measure the air temperature at 5cm and 2m AGL. What we need to know, therefore, is whether and to what extent terrestrial radiation can be determined using these temperature readings only. Because of the difficulties referred to in paragraph 2.1.1 with regard to measuring the net radiation, a distinction is drawn between daytime and night-time measurements. Once the thermal gradient between 2m and 5cm AGL is known, an equation similar to No.16 can be used:

$$E_{5cm} = E_{2m} + \Delta E(O(\Delta T)) = \sigma T_{2m}^4 + 4\sigma T_{2m}^3 (T_{5cm} - T_{2m}) \qquad (19)$$

One can then examine what correction is needed if the only figures available are for the temperature at 2m AGL. Only first order terms expressed in ΔT are important. Figure 10 shows the bias inherent in using the temperature at 2m AGL. By day, the error is appreciably greater than in the case of atmospheric radiation (Figure 9). When there is strong direct radiation, the underestimation may exceed 40 W/m^2. Given equal radiation conditions, it is scarcely influenced by cloud cover. At night, on the other hand, its behaviour is similar to that observed in the case of atmospheric radiation. The signs, of course, are opposite. The clearer the sky, the greater is the overestimation of terrestrial radiation.

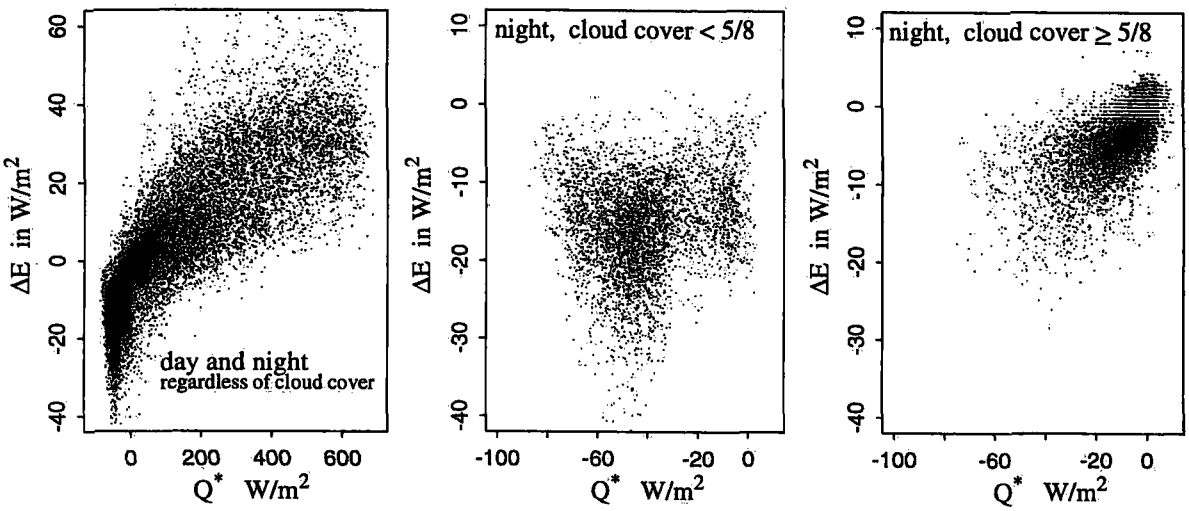

Figure 10. Behaviour of the expression $\Delta E = 4\sigma T_{2m}^3 (T_{5cm}-T_{2m})$ as a function of net radiation

Where measurements of the ground radiation temperature and of the air temperature at 1.1m AGL are available, and where the daytime air temperature is used, Holtslag and Van Ulden (1983) propose a compensatory expression proportional to the net radiation Q^*.

$$E = \sigma T^4 + c_3 Q^* \qquad (20)$$

where $c_3 \cong 0.12$. In their view, this equation is scarcely influenced by cloud cover or wind speed.

4.4.1 Terrestrial radiation at night

A comparison between the measurements taken at night by pyrradiometer and pyrgeometer shows that the figures are in complete agreement. Moreover, a comparison between the measurements and the σT^4 figures calculated using the measured temperature at 5 cm AGL shows that the term σT^4 requires no adjustment. The regression leaves a residual error of 4 W/m^2 and a correlation coefficient of 0.99. This model is therefore perfectly suited to appropriate applications.

If the only measurement available is the temperature at 2m AGL, the adjustment $E = 0.976\,\sigma T^4$ leaves a residual error of approximately 7 W/m^2 and a correlation coefficient of approximately 0.97. Given the nocturnal behaviour illustrated in Figure 10, an equation involving net radiation, similar to equation No.20, would be as follows:

$$E = \sigma T_{2m}^4 + 0.31 Q^* \qquad (21)$$

with a residual error of 6 W/m^2 and a correlation coefficient of 0.98.

A similar approach to that adopted for nocturnal atmospheric radiation (paragraph 4.3.3, equation No.18) has been applied to terrestrial radiation. A large number of tests have shown that the following equation is adequate:

$$E = 0.94\sigma T^4 + 0.12Q^* + 0.24h_{rel} - 30\exp[-(N + \sqrt{u})] \quad (22)$$

Here, humidity plays a role similar to, but less important than, its role in the calculation of atmospheric radiation. However, the determining factor is low wind speed. Equation No.22 leaves a residual discrepancy of less than 4 W/m^2 for a correlation coefficient of 0.99. The coefficients obtained using calculated figures for cloud cover are, in order, 0.95, 0.13, 0.22 and -29, and are thus virtually identical.

4.4.2 Terrestrial radiation by day

The temperature at 5 cm AGL may also be regarded as providing a good approximation of terrestrial radiation by day. Since this measurement instrument is neither ventilated nor shielded from direct solar radiation G, the effect of sunlight on the instrument increases with intensity. The measurements (corrected by equation No.2) provide the following adjustment:

$$E = \sigma T_{5cm}^4 - 0.024G \quad (23)$$

If use is made of the air temperature, generally measured at 2 m AGL in accordance with the WMO convention, the coefficients of the following equations will be adopted.

$$E = \sigma T_{2m}^4 + 0.043Q^* \quad \text{or} \quad E = \sigma T_{2m}^4 + 0.027G \quad (24)$$

To preserve the same form of equation for calculating net radiation both by day and at night, version E(Q*) will be used.

4.5 Net radiation

Figure 11 shows the daily variation in net radiation Q* for a completely clear day in winter or summer, and the distribution of its measured values (corrected COMRAD measurements) at night ($G \leq 5$ W/m^2) and during the day for the years 1988 to 1990.

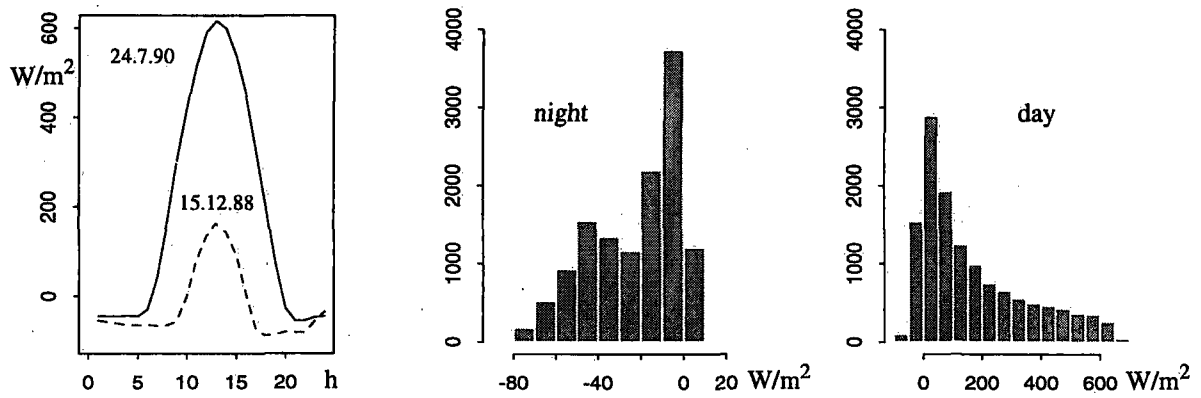

Figure 11. Net radiation: Daily variation under clear weather conditions, with night and daytime distributions given in absolute frequency (three years)

On a clear night, net radiation figures may approach -90 W/m^2 in winter and -70 W/m^2 in summer during the early hours of the night. The night-time distribution is bimodal. This shows that heat loss from the ground by radiation increases rapidly when the sky is sufficiently clear. Roughly

speaking, therefore, total cloud cover may be divided into two categories - one of less than and the other of more than 4/8. Nevertheless, this is still an arbitrary cut-off point, given the subjective nature of cloud observation at night. The average figure for net radiation at night under clear skies (cloud cover $\leq$ 3/8) is -42 W/m^2; when the sky is cloudy (cloud cover 4/8 or more) the figure is -13 W/m^2. The daytime distribution is given here only to show how the two distributions compare when we choose to separate the daytime and night-time periods by a cut-off value of 5 W/m^2 for the measured global radiation G.

4.5.1 Summary of the various ways of calculating net radiation

To calculate the net radiation at night and by day, one must at least know the temperature at 2 m AGL and the cloud cover. If cloud cover is not observed locally, observations made (eight times a day) at the nearest synoptic station may be used, as long as this station is located within the same topographical entity. At present, many ANETZ stations carry out a reduced programme of cloud cover observation but take continuous measurements of wind speed, global radiation G, the temperature at 2 m and 5 cm AGL and of the humidity and precipitation, so that the cloud cover can be estimated. Thus, on the basis of the various equations for calculating atmospheric and terrestrial radiation, as set out in the earlier paragraphs of this chapter, there are eight different ways of calculating the net radiation Q* as defined by equation No.9. These "variants" are summed up in Table 5 below:

Table 5. Variant ways of calculating net radiation

variants	1	2	3	4	5	6	7	8
temperature	2m, 5cm	2m, 5cm	2m, 5cm	2m, 5cm	2m	2m	2m	2m
cloud cover	observed	calculated	observed	calculated	observed	calculated	observed	calculated
equations	25	25	18, 25	18, 25	27	27	28	28

Table 6. Coefficients for calculating net radiation

	r	a	b	c_2	c_3
night	----	0.000288	1.408	56	0.310
day	0.24	0.00342	0.959	58	0.043

The different coefficients, which are common to the equations referred to in Table 5 under the heading "observed cloud cover" but are specific to night-time and daytime periods, are set out in Table 6. Values a and b correspond to the cloud cover calculated using the method adopted in paragraph 3.2. Where the cloud cover is actually observed, the values a and b are given in Table 4.

4.5.2 Calculation using temperatures at 2m and 5m above ground level

Most of the ANETZ stations supply figures for the temperature at 5cm AGL and for global radiation G. The temperature is measured above a lawn or other grassy surface. If the total cloud cover N is not observed, it must be determined using the "modified Albisser" method described in Annex 2. The following equation is derived from equations 12, 17 and 23.

$$Q^* = (1.024 - r)\,G + c_1\sigma T_{2m}^4 - \sigma T_{5cm}^4 + c_2 N \qquad \text{where} \qquad c_1 = aT^b \qquad (25)$$

Table 7 shows the extent to which the figures match the (corrected) measurements, at night and by day. The figures in brackets are those obtained using the observed cloud cover. The result is

slightly improved by using equation No.18 to calculate the nocturnal atmospheric radiation.

Table 7. Net radiation and its components: coefficients of correlation between measurements and calculations

Components	W	$W_{1)}$	E	Q^*	$Q^*_{1)}$
day	0.85 (0.83)	----	0.99	0.99 (0.99)	----
night	0.89 (0.89)	0.91 (0.92)	0.97	0.61 (0.56)	0.72 (0.69)
day and night	0.87 (0.86)	0.87 (0.88)	0.98	0.99 (0.99)	0.99 (0.99)
1) Nocturnal component calculated using equation No.18 instead of No.17					

Although components W and E can, in general, be fairly accurately calculated by parametrization, it is clear that the differences between their calculated nocturnal values do not correlate at all well with the values measured. One reason for this, of course, is that the night-time figures for net radiation lie within a smaller range but are not influenced by any particularly dominant factor. Moreover, equation No.26 (Stahel, 1993) shows that the poor correlation of the night-time values for net radiation Q^* is due to the fact that the differences between the residuals (indices R) of W and E (i.e. $Q^*_R = W_R - E_R$) are too often about as large as the values of Q^* itself. There is no direct theoretical link between the correlation coefficients (measurement, model) r_{Q^*}, r_W and r_E, but r_{Q^*} is determined solely by the behaviour of the Q^*_R residuals (correlation r and variance σ^2).

$$r^2_{Q^*} = \frac{\left(1 + r\left(Q^*_{mod}, Q^*_R\right)\sqrt{\frac{\sigma^2\left(Q^*_R\right)}{\sigma^2\left(Q^*_{mod}\right)}}\right)^2}{1 + 2r\left(Q^*_{mod}, Q^*_R\right)\sqrt{\frac{\sigma^2\left(Q^*_R\right)}{\sigma^2\left(Q^*_{mod}\right)}} + \frac{\sigma^2\left(Q^*_R\right)}{\sigma^2\left(Q^*_{mod}\right)}} \qquad (26)$$

This equation may be simplified to $0.5\left(1 + r\left(Q^*_{mod}, Q^*_R\right)\right)$ where the residuals vary in a particular field by roughly the same amount as the value of Q^* itself. In fact, given the observed cloud cover at night $r\left(Q^*_{mod}, Q^*_R\right) = -0.38$, and $\sigma^2\left(Q^*_R\right) \cong \sigma^2\left(Q^*_{mod}\right)$, the resulting value for $r_{Q^*} = 0.56$. At night, using calculated figures for the cloud cover, the variance of the residuals remains the same whereas the variance of the calculated totals is reduced (the model gives a smaller distribution) which of itself weakens the correlation. But since $r\left(Q^*_{mod}, Q^*_R\right) = -0.056$, equation No.26 gives $r_{Q^*} = 0.63$, which is a slightly better result than in the case of observed cloud cover.

4.5.3 Calculation using only the temperature at 2m above ground level

All conventional weather stations measure the temperature at 2 m AGL, either three or eight times a day. If these are the only figures available, equations 12, 17 and 20 may be applied and Q^* may be calculated as follows:

$$Q^* = \frac{(1-r)\,G + (c_1 - 1)\,\sigma T^4_{2m} + c_2 N}{1 + c_3} \qquad (27)$$

Factors c_1, c_2 and c_3 are to be taken from Table 6.

When this is combined with equations 18 and 22, which are more specific to the situation at night, the results is as follows:

$$Q^* = \frac{(1-r)G + (0.82c_1 - 0.94)\sigma T^4 + c_2 N + c_4 h_{rel} + c_5 \exp[-(N+\sqrt{u})]}{1+c_3} \qquad (28)$$

with the following modified coefficients:

$0.82c_1$, $c_2 = 48$, $c_3 = 0.12$, $c_4 = 0.42$ and $c_5 = 41$ in the case of observed cloud cover,
$0.84c_1$, $c_2 = 63$, $c_3 = 0.12$, $c_4 = 0.13$ and $c_5 = 86$ in the case of calculated cloud cover.

This change in the values of the coefficients is also due to the fact that the Albisser method used for calculating the cloud cover takes into account the humidity and wind speed. The term (1-*r*)G in equation No.28 may seem superfluous, but since the cut-off point between day and night is set at G=5W/m^2, the first and last hours of the night at not automatically disregarded.

Table 8. Net radiation and its components: coefficients of correlation between measured and calculated values

Components	E	$E_{1)}$	Q^*	$Q^*_{1)}$
day	0.98	----	0.99 (0.99)	----
night	0.98	0.99 (0.99)	0.69 (0.69)	0.77 (0.78)
day and night	0.99	0.99 (0.99)	0.99 (0.99)	0.99 (0.99)

1) Nocturnal component calculated using equation No.22 instead of No.21, or 28 instead of No.27

The degrees of correspondence between calculated and measured values are given in Table 8. Those relating to atmospheric radiation have already been given in Table 7. Paradoxically, although the correlations are just as good by day, they are better at night (0.69) than when using the temperature at 5 cm AGL. There is reason to think that variations in temperature near ground level are not all due to factors which influence net radiation.

4.5.4 Comparison of the distributions of calculated and measured net radiation

Figure 12 shows the characteristics of the distributions of net radiation at night and of the residual discrepancies in the eight variants set out in Table 5. The central dark rectangle contains 50% of the values. The median, shown by a white mark, gives an indication of the asymmetry of the nocturnal net radiation distribution. As we have already seen in Figure 11, these are in fact bimodal distributions. The vertical dotted lines show the range of values. The length of these lines is never more than 1.5 times the length of the central rectangle. The most extreme values are shown in isolation.

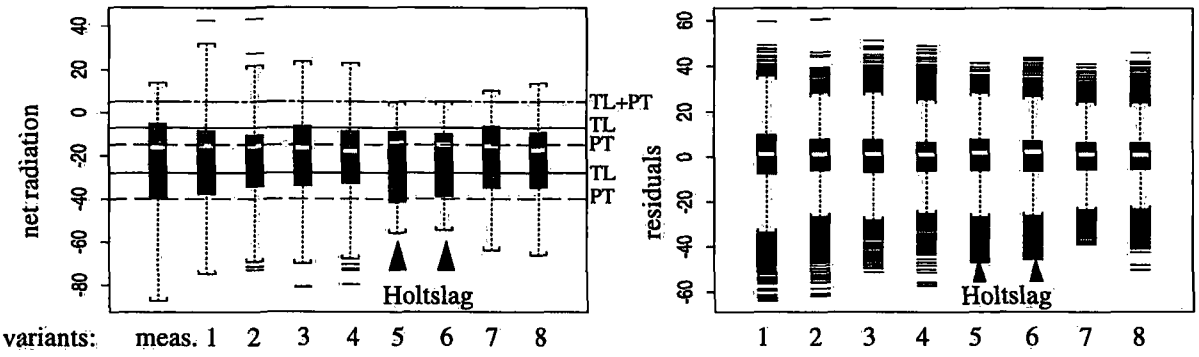

Figure 12. Characteristics of the distributions of calculated net radiation at night compared with the measured values
left: distributions of the measured values and of the eight variants
right: distributions of the residual values of the eight variants.

The horizontal lines in the left-hand graph show the net radiation class limits taken from the TAluft (TL) and Pasquill-Turner (PT) adaptation tables given in Annex 1. A direct comparison between distributions obtained using the 8 variants and the distribution of the measured values is given in Annex 4. As a whole, the variants - and in particular the simple model produced by Holtslag - reproduce rather poorly the extreme values for net radiation measured under clear sky conditions.

The residual values follow a gaussian distribution, with variants 7 and 8 giving the smallest standard deviation (10 W/m^2) and variant 1 giving the largest (15 W/m^2). Nevertheless, the residual values of variants 1, 2, 5 and 6 show a seasonal variation which is eliminated by adding the exponential term (equations 18 and 28) found in variants 3, 4, 7 and 8.

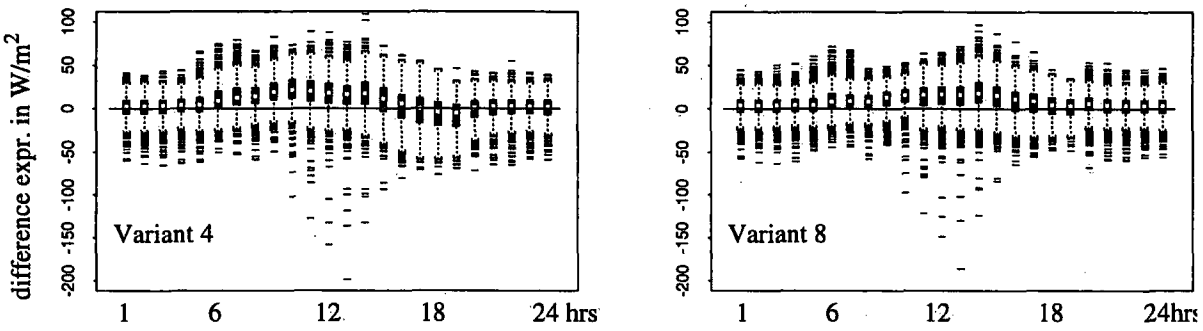

Figure 13. Daily behaviour of the distributions of the differences between the net radiation as measured and as calculated using Variants 4 and 8 (see Table 5)

As with Variants 4 and 8, Figure 13 shows that the model overestimates the daytime net radiation. In the case of the values given for the middle of the day, this error is due to the fact that the albedo *r* has been given a constant value of 0.24. If the daily variation in albedo is introduced, as proposed in equation No.10, it corrects this discrepancy: but this does not explain the over-estimation of the values calculated for the early hours of the day, especially in Variant 4. If the day/night cut-off point is set at a value exceeding 5 W/m^2, only a partial improvement results. Further investigations will be necessary, but we shall not undertake them here.

4.5.5 Net radiation and its applications

In this study, net radiation is essentially used for the purposes of classifying atmospheric stability, or more specifically for calculating dispersion categories as defined in Annex 1: but it is also a crucial factor in calculating the energy budget near ground level as described in equation No.29:

$$H + H_L = Q^* - H_S \qquad (29)$$

This equation shows that the radiation which contributes to the sensible heat flux H and latent heat flux H_L is equal to the net radiation less the ground heat flux H_S. As an approximation, H_S may be regarded as proportional to Q^*, and the resistance method proposed by Monteith (1990) may be used to determine H and H_L. Holtslag (1983) has compiled the coefficients needed for this calculation. If the sensible heat flux H is known, the Monin-Obukhov similarity theory makes it possible to determine the friction velocity u^* and the Monin-Obukhov length L (stability factor) which are related by the equation $L = A\frac{Tu^{*3}}{H}$. These parameters are needed for estimating the height of the mixing layer. Unfortunately, only ideal cases of nocturnal temperature inversion can be calculated on this basis (Stull, 1989).

5. SUMMARY AND CONCLUSIONS

The two parameters required for calculating the stability or state of turbulence of the atmosphere near ground level are net radiation and wind speed. Although wind speed is measured at many stations in Switzerland net radiation is measured only rarely. This study shows how net radiation may be estimated on the basis of measurements and observations carried out by the ANETZ network and may then be used for determining dispersion categories.

The results of this study are based on two measurement projects undertaken at Payerne, one common feature of which is the aim of testing the equipment used for measuring different radiation components. Considerable inaccuracies in certain measurements had to be corrected at a relatively late stage in the study. Some of the corrections set out in this report relate specifically to instruments used in the COMRAD project, and cannot normally be applied to other instruments of the same type.

A simple parametrization of net radiation proposed by Holtslag and Van Ulden (1983) was tested separately on daytime and night-time periods. A few additions made it possible to improve the night-time model by eliminating, in particular, systematic effects of seasonal variations. There is also good reason to take account of a daily variation in albedo under clear weather conditions throughout the year, although its cause (type of ground surface or instruments used etc.) has not yet been established.

Observed cloud cover is not an ideal meteorological datum for calculating net radiation. Where cloud cover is not actually observed, the night-time situation may be estimated using the Albisser (1983) method and the daytime situation using the Kasten (Holtslag and Van Ulden, 1983) method. Both these methods have been tested. Sunshine duration measurements may be used instead. We have proposed modifications which somewhat improve the results. Nevertheless, the day-night transition periods are still the most difficult ones to model because of the uncertainties in the alternative parameters available, particularly the difference in temperature between 2m and 5cm above ground level. As with the Albisser figures for estimated cloud cover at night, the equations set out in Chapter 3 of this study should be "adjusted" to the conditions prevailing at the other ANETZ stations.

Net radiation is an essential factor in calculating the energy budget at ground level. When it is known, other important parameters such as heat fluxes, the friction velocity, the Mornin-Obukhov length and, finally, the height of the mixing layer can be calculated.

Acknowledgements

I would like to thank my colleagues at SMI for their help with this study, and in particular Dr. A. Zelenka for his help in the field of radiation. My discussions with Mr. P. Wasserfallen and Dr. A. Heimo, the scientists responsible for the COMRAD and BSRN projects at Payerne, and the figures made available from their projects, enabled me to carry out the adjustments which feature so prominently in this report. Dr. R. Stubi, Dr. D. Cattani and Mr. P. Jeannet were kind enough to re-read the entire report, and I would like to thank them for their constructive comments and suggestions. Since nothing nowadays can be done without an efficient data processing system, I would also like to thank all those colleagues who have done such a good job on the computer front.
This English translation of my original French version was provided by the Translation Service of the European Commission in Brussels for the purpose of the COST-Action 710. I express my gratitude to the above mentioned Translation Service for its very useful work.

Author's address:
Philippe Tercier
Swiss Meteorological Institute
Les Invuardes
CH-1530 Payerne

6. REFERENCES

Albisser P., 1983: Abschätzung der nächtlichen Gesamtbewölkung mit Hilfe von ASTA-Daten. *Working Reports of the SMI*, No 116, Zürich, 50p.

Bosshard W., 1992: Parametrisierung der Wolkentransmission basierend auf ANETZ-Daten für die Wolkentypen Cirrus, Altocumulus, Stratus, Cumulus. Diploma work. Swiss Federal Institute of Technology GGIETH, Zurich. 108p.

Bundesminister der Justiz BRD, 1987: Richtlinie zur Durchführung von Ausbreitungsrechnungen nach TALuft mit dem Programmsystem AUSTAL86, *Bundesanzeiger,* 131a, 288p.

Culf A.D. and J.H.C. Gash, 1993: Longwave Radiation from Clear Skies in Niger: A Comparison of Observations with Simple Formulas. *J. Appl. Meteor.*, **32**, 539-547.

D'Agostino V. and A. Zelenka, 1992: Supplementing Solar Radiation Network Data by Co-kriging with Satellite Images. *Int.J.of Climatology,* **12**, 749-761.

Davies J.A., Mckay D.C., Luciani G. and M. Abdel-Wahab, 1988: Validation of models for estimating solar radiation on horizontal surfaces, Final Rept. for IEA Solar Heating and Cooling Programme Task 9, Phase I, Subtask B. Canadian Climate Centre, Atmosphere Environment Service, Downsview, Ontario M3H 5T4. 99p.

Filliger P. and U. Nyffeler, 1993: Le nouveau réseau national d'observation des polluants atmosphériques (NABEL) est opérationnel. *Bulletin of FOEFL,* 1/93, Berne, 21-27.

Hächler P., 1993: Konzept Netze 93, *Working Reports of the SMI*, No 181, Zürich, 39pp..

Heimo A., 1990: Durée d'insolation, II : Mesures de l'influence du seuil de sensibilité. *Working Reports of the SMI*, No 158, Zürich, 52p.

Henselder R., 1986: TALuft Vorschriften zur Reinhaltung der Luft, Einleitung und Erläuterungen. *Bundesanzeiger,* 152p.

Holtslag A.A.M. and A.P. Van Ulden, 1983: A Simple Scheme for Daytime Estimates of the Surfaces Fluxes from Routine Weather Data. *J. Appl. Meteor.*, **22**, 517-529.

Idso S.B. and R.D. Jackson, 1969: Thermal Radiation from the Atmosphere. *J. Geoph. Res.*, **74**, 5397-5403.

Monteith J.L. and M.H. Unsworth, 1990: Principles of Environmental Physics, 2. edition. *E. Arnold.*

OMM, 1990: Guide des instruments et des méthodes d'observation météorologiques. 5.edition.

OMM, 1991: Radiation and Climate (Second Workshop on Implementation of the Baseline Surface Radiation Network, Davos, Switzerland, 6-9 August 1991) WCRP-64, (WMO/TD-No.453).

Paltridge G.W. and C.M.R. Platt, 1976: Radiative Processes in Meteorology and Climatology. Development in Atmospheric Science. Vol.5, *Elsevier.*

Pasquill F. and F.B. Smith, 1983: Atmospheric diffusion. *Ellis Horwood limited,* 3. edition (1.ed.,1962)

Polster G., 1969: Erfahrungen mit Strahlungs-, Temperaturgradient- und Windmessugen als Bestimmungsgrössen der Diffusionskategorien. *Met. Rundschau,* **22**, 170-175.

Stahel W., 1993: Personal communication , Seminar for Statistic, Swiss Fed. Inst. of Technology, Zürich.

Statsci, 1991: S-PLUS Reference Manual,version 3.0, Statistical Sciences, Inc. Seattle, Washington.

Stull R.B., 1989: An Introduction to Boundary Layer Meteorology, *Kluwer Academic Publishers*, Dordrecht, The Netherlands.

Turner D.B., 1964: A Diffusion Model for an Urban Area. *J. Appl. Meteor.*, **3**, 83-91.

Wasserfallen P., 1991: Projet COMRAD (COMparaison de RADiomètres), Descriptif et premier bilan. Internal Report, Deprt.. of environmental meteorology, SMI, Payerne., 26p.

Zelenka A., Bantle H. and D. Lazic, 1991: Horizonts apparents ainsi qu'arcs diurnes calculés et observés pour les héliomètres du réseau ANETZ de l'ISM. *Working Reports of the SMI*, No 166, Zürich, 59pp.

Zelenka A., Czeplak G., D'Agostino V., Josefsson W., Maxwell E., Perez R., Noia M., Ratto C. and R. Festa, 1992: Techniques for Supplementing Solar Radiation Network Data. A Report of Task 9: Solar Radiation and Pyranometry Studies. Vol. 1-3. International Energy Agency, Solar Heating & Cooling Programme. Report No. IEA-SHCP-9D-1.

Annex 1

Schemes for identifying the classes of atmospheric stability (or dispersion categories) on the basis of measurements taken by the ANETZ network Adaptation of the Pasquill-Turner and TALuft schemes

A 1.1 Preliminary remarks

The combined effect of wind and heat flux on atmospheric turbulence is taken into account when defining dispersion categories (or stability classes). The schemes used for defining dispersion categories use a precise combination of meteorological measurements from which one should, in principle, not stray too far. For example, the wind speed has been measured 10 m AGL, or the temperature gradient is based on measurements taken over a vertical distance of 100 m. On the other hand, the wind speed measurement used for establishing the wind distribution under the conditions of a particular predetermined stability class maybe taken at a different height above ground level. In any case, dispersion models adapt, or should adapt, the wind speed value to the actual height of the smoke plume, or at least to the height of the chimney.

A 1.2 Original schemes

The schemes distinguish, in general, 6 or 7 classes of atmospheric stability which are designated by the letters A to F (or G) and are defined as follows:

Class A :	very unstable	Class B :	unstable
Class C :	slightly unstable	Class D :	neutral
Class E :	stable	Class F :	very stable

For the sake of simplicity, these classes may be grouped in pairs A-B, C-D and E-F.

A 1.2.1 Pasquill-Turner

The method devised by Pasquill in the 1960s (Pasquill and Smith, 1983) is still widely used. For a long time it was the only method whereby the atmosphere's dispersion characteristics could be deduced from widely available meteorological parameters, since these were the usual synoptic data and observations. In particular, Pasquill analyzed the fluctuation in wind speed and direction at 10 m AGL, and correlated this data with the thermodynamic state of the lower atmosphere.

Table A1. Determination of dispersion categories according to Pasquill

Wind speed at 10 m (m/s)	DAY			NIGHT	
	Incident solar radiation			Incident solar radiation moderately overcast: cloud cover between 4/8 and 7/8	cloud cover ≤ 3/8
	Strong	Moderate	Weak		
<2	A	A-B	B	F	F
2–3	A-B	B	C	E	F
3–5	B	B-C	C	D	E
5–6	C	C-D	D	D	D
>6	C	D	D	D	D

By day, his **dispersion categories** (Table A1) are determined on the basis of the wind speed measured at 10 m AGL and the intensity of the solar radiation. At night (from 1 h before sunset to 1 h after sunrise), he uses wind speed and cloud cover. Radiation classes are defined as follows:

- Under clear weather conditions (cloud cover $\leq$ 3/8), the incident solar radiation is strong when the elevation of the sun is $\geq$ 60° ; it is moderate when this elevation is between 60° and 35° and it is weak when the elevation is between 35° and 15° .
- When the sky is moderately overcast (cloud cover between 4/8 and 7/8), the same elevations of the sun give the lower radiation category.
- When the sky is completely overcast, the radiation is categorized as Class D, by night and day, regardless of wind speed.

Turner (1964) introduced a radiation index which took account of the sun's elevation and the cloud cover. Moreover, if measurements of the global radiation G are available, the following classification is proposed:

Strong radiation	$G \geq 600$ W/m^2
Moderate radiation	$300 < G < 600$ W/m^2
Weak radiation	$G \leq 300$ W/m^2

A 1.2.2 TALuft

Dispersion categories are also based on synoptic meteorological data. They take into account the wind speed at 10 m AGL, the cloud cover, the type of cloud and the time of year. This scheme was drawn up on the basis of analyses of the correlation between various meteorological parameters measured near ground level in Germany in the 1960s and 1970s. Disregarding the position of the sun meant introducing a number of conditions to take account of the time of year, and this makes the structure of the scheme rather complicated. Three sets of dispersion coefficients are available depending on the actual height of the smoke plume (50 m, 100 m, >150 m). The scheme and the values of the coefficients form part of the German TALuft Directives. They appear in the document published by the Bundesminister der Justiz BRD (1987) on the AUSTAL86 gaussian dispersion model which implements the TALuft Directives to the letter, and in a work published by Henselder (1986).

A 1.2.3 Polster

Given the figures for the temperature measured at different heights above ground level and for the net radiation at Jülich (Germany), Polster (1969) established the correlations between these figures and the synoptic parameters proposed by Pasquill. He thus drew up the following scheme (Table A2) for classifying dispersion categories in accordance with each of these two parameters.

Table A2. Determining dispersion categories on the basis of the temperature gradient, net radiation and wind speed (after Polster, 1969)

Wind speed u (m/s)	Temperature gradient (°C/100m) between 120 and 20 m AGL						
	≤ - 1.5 very unstable	- 1.4 ... - 1.2 medium instability	- 1.1 ... - 0.9 slight instability	- 0.8 ... - 0.7 neutral	- 0.6 ... - 0.0 slight stability	0.1 ... 2.0 medium stablility	> 2.0 very stable
	Net radiation Q* (cal/cm2min) Q*> 0 : resultant incident downward radiation Q*< 0 : resultant radiation emitted upwards						
	> 0.60 strong	0.60 ... 0.35 medium	0.34 ... 0.16 weak	0.15 ... 0.09 very weak	0.08 ... - 0.01 neutral	- 0.02 ... - 0.04 medium	£ - 0.05 strong
0.0 - 0.9	A	A	B	C	D* (E)	G	G
1.0 - 1.9	A	B	B	C	D* (D)	G	G
2.0 - 2.9	A	B	C	D	D	E	F
3.0 - 4.9	B	B	C	D	D	D	E
5.0 - 6.9	C	C	D	D	D	D	E
≥ 7.0	D	D	D	D	D	D	D

The wind data used by Polster were measured at 20m AGL, but when allowance is made for the effects caused by obstacles this is equivalent to a height of 10m AGL. The net radiation is given in cal/cm2 min, and the factor for transformation into W/m^2 is 698. The temperature gradient and the net radiation are not easy to measure. In Switzerland, nuclear power plants have tall weather masts which make it possible to measure the temperature gradient. Some SMI stations known as "surface layer" stations supply, or will supply, figures for this parameter. If measurements are taken at elevations below 100m, extreme categories gain in importance since the differences are greater close to the ground. The temperature gradient measured on a slope can be used, provided precautions are taken with the extent to which the measuring instruments are exposed. Measurements obtained under these conditions tend to underestimate extreme classes. Measuring net radiation is difficult and requires careful control. To simplify application of the Polster scheme, Class D*, (which was not defined by Polster in relation to the dispersion coefficients) has been renamed E or D as indicated in Table A2. Finally, categories F (exceptional in the Polster scheme) and G have been put together in a single class F, since the German TALuft Directives (Henselder, 1986) provide dispersion coefficients for six classes only.Finally, categories F (exceptional in the Polster scheme) and G have been put together in a single class F, since the German TALuft Directives (Henselder, 1986) provide dispersion coefficients for six classes only.

A 1.3 Schemes adapted by the SMI

The Polster scheme requires parameters which are not measured by weather station networks such as the ANETZ network operated by the SMI. The conventional schemes use figures for the cloud cover, which is observed with sufficient frequency (every three hours, day and night) at only a few of the main stations known as "synoptic" stations. Other stations observe the cloud cover only three times a day - at 7.00, 13.00 and 19.00 hours - which is insufficiently frequent for the temporal (and thus spatial) interpolation of figures. It has therefore proved necessary to establish a scheme for determining atmospheric dispersion categories using the hourly data provided by the ANETZ network. We are aiming to find the best possible statistical correspondence with the TALuft scheme or the Pasquill-Turner scheme so as to find an acceptable way of making widespread use of the dispersion coefficients which are closely linked to these schemes.

Initially, in order to meet demand as quickly as possible, the idea was to find a simple way of parametrizing net radiation by day and at night so that the Polster scheme could be applied. In the first instance, analysis of the hourly figures for global radiation G shows that it is sufficient for the purposes of establishing the day/night cut-off point, i.e.:

$$\text{day: } G > 5 \text{ W/m}^2 \qquad \text{night: } G \leq 5 \text{ W/m}^2$$

Daytime net radiation:

Hourly measurements were taken over a three year period (November 1987 to October 1990). When these figures are used without the correction proposed in paragraph 2.1.1, the correlation between net radiation Q* as measured by the COMRAD project and global radiation G as measured by the ANETZ station yields the regression which was initially adopted:

$$Q^* = -13.06 + 0.60\, G$$

where the residual error of 50 W/m^2 is still considerable. This error is partly due to the time gap between the two measurements Q* and G. If account is taken of the correction made to the net radiation measurement, and if this measurement is correlated with the synchronized measurement G (COMRAD), the result is

$$Q^* = -17.6 + 0.61\, G + 0.0001\, G^2$$

with a residual error of 30 W/m^2.

Nocturnal net radiation:

There is a clear statistical trend in the relationship between net radiation and the temperature difference between 2m and 5cm AGL (Δt). Over the three years during which measurements were taken, this trend may be described by the following linear equation:

$$Q^* = - 10.79 - 10.36\ \Delta t$$

The residual error of 16 W/m^2 is nevertheless fairly large. Since the COMRAD project did not include the temperature measured at 5cm AGL, temperature measurements taken by the ANETZ station were used, and this implies a time lag between the measurements.

The next step was to compare, over a twelve month period (December 1988 - November 1989), the atmospheric stability calculated by the original Pasquill-Turner and TALuft schemes with the stability figures provided by the Polster scheme and the equations set out above, and then to define such modifications as might be necessary to the classes of net radiation Q^*, of temperature difference and of wind speed u measured at 10m AGL, so that the frequency of each stability class was as close as possible to that of the original schemes. This exercise showed that the differences between the two schemes (Pasquill and TALuft) were too great to allow these schemes to be replaced by a single alternative scheme. Furthermore, it is important to ensure that the dispersion coefficients adopted as the basis for these schemes continue to be used in a homogeneous fashion. Pasquill-Turner reflects atmospheric dispersion experiments carried out on the vast plains of America, whereas TALuft is the result of experiments made in Germany at Jülich and Karlsruhe under very different conditions. The analysis thus yielded the following two adaptations.

A 1.3.1 Adaptation of the Pasquill-Turner scheme

The scheme given in Table A3 originates in the scheme drawn up by Polster (Table A2) using net radiation and wind speed. The changes made to the classes of net radiation Q^*, the new designation of some cells in the Table (< >) and the changes to the way in which class limits are set for the temperature difference between 2m and 5cm AGL are the result of the correlation carried out between these categories and those established under the Pasquill-Turner scheme (Pasquill and Smith, 1983) on the basis of cloud cover. For each stability class, the following (unmodified) frequencies of correspondence have been established between the Pasquill-Turner calculation and that given in Table A2 (D^* modified), with the net radiation equations given in paragraph A1.3:

Stability class	A	B	C	D	E	F
	83	65	28	47	36	91 %

This result shows that 91% of the cases assigned to Class F under the Pasquill-Turner scheme are also designated as such by the substitute scheme, but that only 28% of the cases assigned to Class C are similarly designated under the substitute scheme. The "Polster" wind speed classes have had to be modified. It should be noted that at Jülich, to allow for the effect of obstacles, the wind speed was measured at 20m AGL and these figures have been corrected only approximately to bring them into line with those measured at 10m AGL. Given the configuration of Table A3, the correspondence frequencies for the different stability classes are:

Stability class	A	B	C	D	E	F
	76	76	53	65	55	77 %

Table A3. Determining the dispersion categories: substitute scheme adapted from Pasquill-Turner

Q: (W/m^2) ΔT: (K)	> 460	460 - 240	240 - 110	110 - 5	5 - -15 ≤ 1.0	-15 - -40 1.0 - 2.2	≤ -40 > 2.2
u: 0.0 0.7	A	<B>	B	C	<F>	<F>	<F>
0.8 1.4	A	B	B	C	<D>	<F>	<F>
1.5 2.9	A	B	C	D	D	E	F
3.0 4.4	B	<C>	C	D	D	<E>	E
4.5 5.9	C	C	D	D	D	D	<D>
≥ 6.0 (m/s)	D	D	D	D	D	D	D

< > different from what appears in the original Polster scheme (1969)

A 1.3.2 Adaptation of the TALuft scheme

The adaptation procedure is similar to that applied to the Pasquill-Turner scheme. Given their origins, the Polster and TALuft schemes resemble each other much more closely than they do the Pasquill-Turner scheme. For each stability class, the following (initial) frequencies of correspondence have been established between the TALuft calculation and that given in Table A2 (D^* modified), with the net radiation equations given in paragraph A1.3:

Stability class	A	B	C	D	E	F
	53	57	26	54	24	92 %

No alteration to the wind speed classes was necessary to improve the correspondence, and only a small adjustment was made to the net radiation classes. The class limits for the temperature difference between 2m and 5cm are lower than in the Pasquill scheme. It was, however, necessary to rename some of the cells in the Table (< >). Given the new configuration (Table A4), the correspondence frequencies for the different stability classes are:

Stability class	A	B	C	D	E	F
	70	59	59	62	56	86 %

If Classes A and B, C and D, E and F are taken together, the resulting correspondence frequencies are 84, 76 and 86%.

Table A4. Determining the dispersion categories: substitute scheme adapted from TALuft

Q: (W/m^2) ΔT: (K)	> 390	390 - 240	240 - 80	80 - 5	5 - -7 ≤ 0.6	-7 - -28 0.6 - 1.5	≤ -28 > 1.5
u: 0.0 0.9	A	A	B	C	<E>	<F>	<F>
1.0 1.9	A	B	B	C	<E>	<E>	<F>
2.0 2.9	A	B	C	<C>	D	<D>	<E>
3.0 4.9	<A>	B	C	<C>	D	D	<D>
5.0 6.9	<B>	C	D	D	D	D	<D>
≥ 7.0 (m/s)	D	D	D	D	D	D	D

< > different from what appears in the original Polster scheme (1969)

Annex 2

Algorithms for estimating total cloud cover

Symbols RR = precipitation, h_{rel} = relative humidity, u = wind speed in m/s
G = global radiation at 2 m AGL, S = sunshine duration
Δt = temperature difference between 2 m and 5 cm AGL
N = total cloud amount expressed in eighths
ϕ = elevation of the sun

night : $G < 5$ W/m^2 and $\sin\phi \leq 0.05$, "**Albisser**" method

if RR = 0 and $\Delta t \leq 0$ and $h_{rel} \geq 94.5$ and $u \leq 1.2$
then **N = 9**
if RR > 0 or ($\Delta t \leq 0$ and $h_{rel} < 94.5$) or ($\Delta t \leq 0$ and $h_{rel} \leq 94.5$ and $u > 1.2$) or ($\Delta t > 0$ and $\Delta t \leq 0.7$)
then **N = 8**
if RR = 0 and $\Delta t > 0.7$ and $\Delta t \leq 1.2$
then **N = 7**
if RR = 0 and $\Delta t > 1.2$ and $\Delta t \leq 1.5$
then **N = 6**
if RR = 0 and $\Delta t > 1.5$ and $\Delta t \leq 1.6$
then **N = 5**
if RR = 0 and $\Delta t > 1.6$ and $\Delta t \leq 1.7$
then **N = 4**
if RR = 0 and $\Delta t > 1.7$ and $\Delta t \leq 2.0$
then **N = 3**
if RR = 0 and $\Delta t > 2.0$ and $\Delta t \leq 2.2$
then **N = 2**
if RR = 0 and $\Delta t > 2.2$ and $\Delta t \leq 2.3$
then **N = 1**
if RR = 0 and $\Delta t > 2.3$
then **N = 0**

night : $G < 5$ W/m^2 and $\sin\phi \leq 0.05$, "**modified Albisser**" method

To bring the figures more closely into line with the distribution of the categories of observed cloud cover N = 1 to 8, the following Δt classes were adopted:

if RR = 0 and $\Delta t \leq 0$ and $h_{rel} \geq 94.5$ and $u \leq 1.2$
then **N = 9**
if RR > 0 or ($\Delta t \leq 0$ and $h_{rel} < 94.5$) or ($\Delta t \leq 0$ and $h_{rel} \leq 94.5$ and $u > 1.2$) or ($\Delta t > 0$ and $\Delta t \leq 0.8$)
then **N = 8**
if RR = 0 and $\Delta t > 0.8$ and $\Delta t \leq 1.3$
then **N = 7**
if RR = 0 and $\Delta t > 1.3$ and $\Delta t \leq 1.7$
then **N = 6**
if RR = 0 and $\Delta t > 1.7$ and $\Delta t \leq 2.1$
then **N = 5**
if RR = 0 and $\Delta t > 2.1$ and $\Delta t \leq 2.4$
then **N = 4**
if RR = 0 and $\Delta t > 2.4$ and $\Delta t \leq 2.6$
then **N = 3**
if RR = 0 and $\Delta t > 2.6$ and $\Delta t \leq 2.9$
then **N = 2**
if RR = 0 and $\Delta t > 2.9$ and $\Delta t \leq 3.2$
then **N = 1**
if RR = 0 and $\Delta t > 3.2$
then **N = 0**

day : $G \geq 5$ W/m^2, "**sunshine duration**" method

if RR = 0 and $\Delta t \leq 0$ and $h_{rel} \geq 94.5$ and $u \leq 1.2$
then **N = 9**
if (RR > 0 and S = 0) or S = 0
then **N = 8**
if (RR > 0 and S > 0
then **N = 7**
if (RR = 0 and S > 0
then **N = 1 - S**
option: Take the average sunshine duration figure
$S = \overline{S}$ (averaged over 3 consecutive hours)
option: Introduce the observed cloud cover data and extrapolate to ± 1 hour
N(6h±1, 12h±1, 18h±1) = observed cloud cover at 6, 12 and 18 hours

day : $G \geq 5$ W/m^2, "**ratio of measured global radiation to global radiation under clear sky conditions**" method

if RR = 0 and $\Delta t \leq 0$ and h_{rel} 94.5 and$u \leq 1.2$
then **N = 9**
if (RR > 0 and S = 0) or S = 0
then **N = 8**
i (RR > 0 and S > 0
then **N = 7**
if (RR = 0 and S > 0
then **N = | 1 - G / G_0 |** **if N > 1.125 then N = 1/N**
option: Take the average ratio of measured global radiation to global radiation under clear sky conditions
$G / G_0 = \overline{G / G_0}$ (ratio averaged over 3 consecutive hours)
option: Introduce the observed cloud cover data and extrapolate to ± 1 hour
N(6h±1, 12h±1, 18h±1) = cloud cover observed at 6, 12 and 18 hours and extrapolated to the preceding and following hours

Annex 3

Calculating the sun's elevation (Holtslag and Van Ulden, 1983)

The number d of the day of the year is determined on the basis of the number M of the month and of the number D of the day of the month, using the following equation:

$$d = 30(M-1) + D$$

If d is known, the longitude of the sun LS (rad.) and its inclination δ are calculated using the following equations:

$$LS = 4.871 + 0.0175d + 0.033 \sin(0.0175d)$$

$$\delta = \arcsin(0.398 \sin(LS))$$

Thus the angle of rotation of the earth h which would bring the meridian from a given longitude west λ to universal time t (expressed in hours) is calculated according to the following equation:

$$h = -\lambda + 0.043 \sin(2LS) - 0.033 \sin(0.0175d) + 0.262t - \pi$$

Finally, for a given latitude ψ (rad.), the sun's elevation ϕ can be calculated, to within 0.05 rad., using the following equation:

$$\sin\phi = \sin\delta \sin\psi + \cos\delta \cos\psi \cos(h)$$

Note that the time lag between universal time t and the local time tl (winter time) at which global radiation is measured can be expressed by the equation t = (tl - 0.5) -1. In the case of ANETZ data, the correction is t = t + 0.17, because of the way in which the data gathering is organized.

Estimating global radiation under clear sky conditions

The coefficients of the following polynomial have been calculated on the basis of the calculated elevation of the sun $\sin\phi$ and of the global radiation measured at the Payerne ANETZ station under clear sky conditions. The residual error is less than 5 W/m^2. The fourth order polynomial is justified on the basis of the different way in which the measurements behave when the sun is low. The cut-off point for this change is approximately $\sin\phi = 0.15$. Subsequently, the figures will be calculated using the following adjustment: an interception factor of 10 instead of 13 so as to correct, to some extent, the discrepancies which occur at low values of $\sin\phi$.

$$G_0 = 13 + 371 \sin\phi + 2226 (\sin\phi)^2 - 2672 (\sin\phi)^3 + 1117 (\sin\phi)^4$$

This equation replaces the two linear equations:

$$G_0 = 569 \sin\phi + 13 \qquad \text{where} \quad \sin\phi < 0.15$$

$$G_0 = 1118 \sin\phi - 69 \qquad \text{where} \quad \sin\phi > 0.15$$

Annex 4

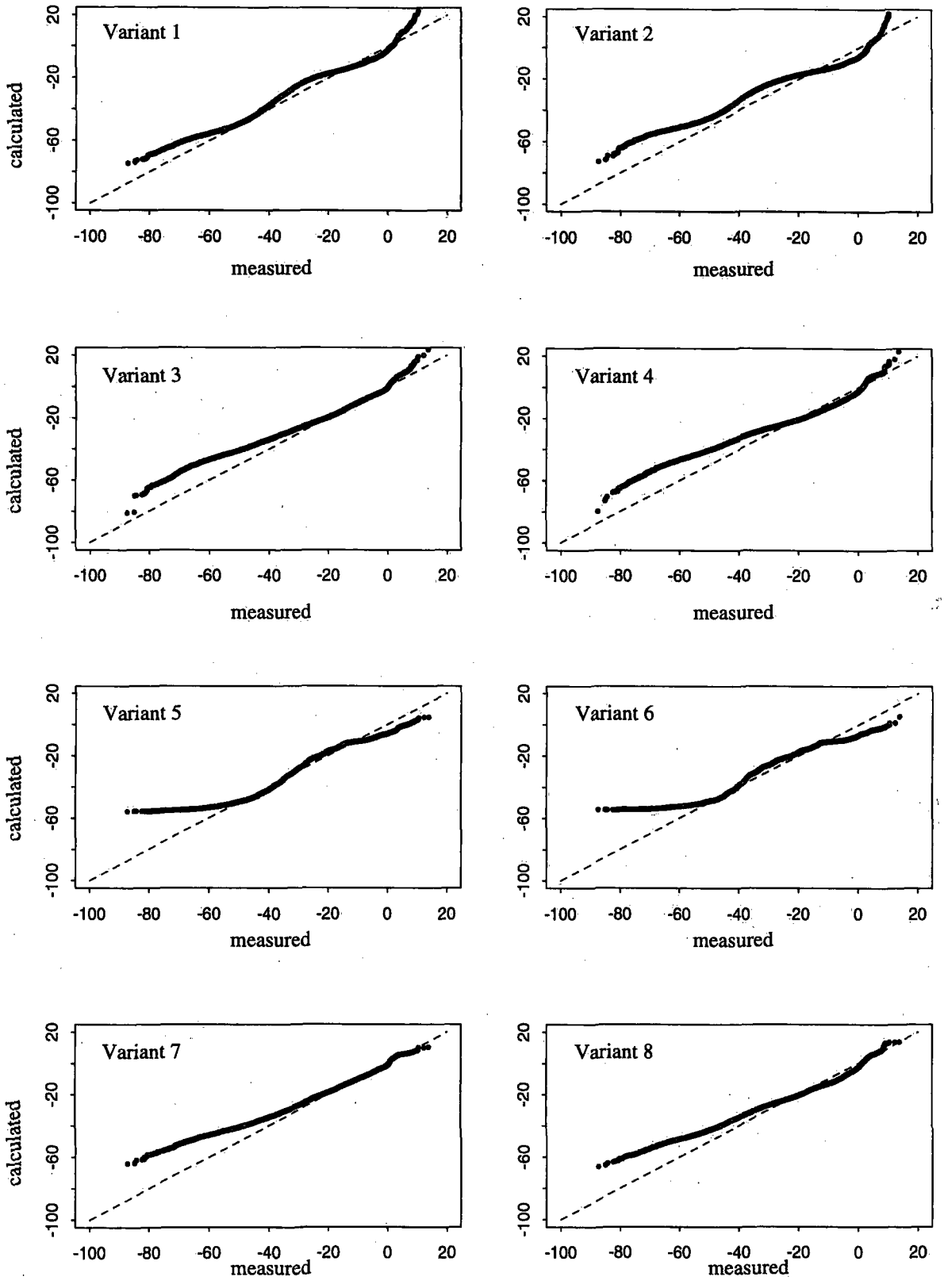

Distributions of nocturnal net radiation, expressed in W/m^2, calculated using variants 1 to 8 (see paragraph 4.5.1, Table 5) compared with the distribution obtained by measurement.

Annex 5

List of stations belonging to the ANETZ network

No ANETZ	NAME	Initials	Coordinates geographical	Coordinates kilometric	Altitude m/asl	Visual obs. (UTC) 00	03	06	09	12	15	18	21	TT ground	TT 5cm	Evap-oration	Type station
1	La Dôle	DOL	46 26 / 06 06	497 050 / 142 380	1670	-	X	X	-	X	-	X	-	-	-	-	SH/GB
2	Payerne	PAY	46 49 / 06 57	562 150 / 184 855	490	X	X	X	X	X	X	X	X	X	X	X	SH/AG/FR/RA
3	Jungfraujoch	JUN	46 33 / 07 59	641 930 / 155 275	3580	-	-	X	X	X	X	X	-	-	-	-	SH/GB
4	Wynau	WYN	47 15 / 07 47	626 400 / 233 860	422	X	X	X	X	X	X	X	X	-	X	-	SN
5	Säntis	SAE	47 15 / 09 21	744 100 / 234 900	2490	-	X	X	X	X	X	X	X	-	-	-	SH/GB/RF
6	Vaduz	VAD	47 08 / 09 31	757 700 / 221 700	460	X	X	X	X	X	X	X	X	X	X	-	SH/AG
7	Aigle	AIG	46 20 / 06 55	560 120 / 130 630	381	-	X	X	X	X	X	X	-	-	X	-	SN/AG
8	Moléson	MLS	46 33 / 07 01	567 740 / 155 175	1972	-	-	-	-	-	-	-	-	-	-	-	GB
9	Fahy	FAH	47 26 / 06 57	562 460 / 252 650	596	X	X	X	X	X	X	X	X	X	X	X	SN/GB/AG
10	Montana	MVE	46 19 / 07 29	603 600 / 129 160	1508	-	-	X	X	X	X	X	-	-	X	-	SN/GB
11	Zermatt	ZER	46 02 / 07 45	624 350 / 097 550	1638	-	-	X	-	X	-	X	-	-	X	-	KB/GB
12	Chasseral	CHA	47 08 / 07 04	571 290 / 220 320	1599	-	-	-	-	-	-	-	-	-	-	-	GB
13	Pilatus	PIL	46 59 / 08 15	661 910 / 203 410	2106	-	-	X	-	X	-	X	-	-	-	-	KB/GB
14	Altdorf	ALT	46 52 / 08 38	690 960 / 191 700	449	X	X	X	X	X	X	X	X	-	X	-	SN/GB/RF
15	Ulrichen	ULR	46 30 / 08 19	666 740 / 150 760	1345	-	-	-	-	-	-	-	-	-	X	-	GB
16	Piotta	PIO	46 31 / 08 41	694 930 / 152 500	1007	X	X	X	X	X	X	X	X	-	X	-	SN/GB
17	Lugano	LUG	46 00 / 08 58	717 880 / 095 870	273	-	-	X	-	X	-	X	-	-	X	-	SN/GB/RF
18	Samedan	SAM	46 32 / 09 53	787 150 / 156 040	1705	-	-	X	X	X	X	X	-	X	X	Y	SN/GB/AG/RF
19	Chur-Ems	CHU	46 52 / 09 32	759 460 / 193 170	555	X	X	X	X	X	X	X	X	X	X	X	SN/GB/AG
20	Napf	NAP	47 00 / 07 56	638 138 / 206 075	1406	-	-	-	-	-	-	-	-	-	-	-	KS
21	Sion	SIO	46 13 / 07 20	592 200 / 118 625	482	X	X	X	X	X	X	X	X	X	X	X	SH/GB/AG/RF
22	Locarno-Magadino	MAG	46 10 / 08 53	711 160 / 113 540	197	X	X	X	X	X	X	X	X	X	X	X	SH/AG
23	Neuchâtel	NEU	47 00 / 06 57	563 150 / 205 600	485	-	-	X	X	X	X	X	-	-	X	-	SN/GB/RF
24	Stabio	SBO	45 51 / 08 56	716 040 / 077 970	353	-	-	-	-	-	-	-	-	X	X	X	KS/AG
25	Interlaken	INT	46 40 / 07 52	633 070 / 169 120	580	X	X	X	X	X	X	X	X	-	X	-	SN/GB
26	Disentis	DIS	46 42 / 08 51	708 230 / 173 780	1190	-	X	X	-	X	-	X	-	-	X	-	SN/GB
27	Hinterrhein	HIR	46 31 / 09 11	733 900 / 153 980	1611	-	-	X	-	X	-	X	-	-	X	-	GB
28	Davos	DAV	46 49 / 09 51	783 580 / 187 480	1590	-	-	X	-	X	-	X	-	X	X	Y	KB/GB/AG/RF
29	St.Gallen	STG	47 26 / 09 24	747 940 / 254 600	779	-	-	X	X	X	X	X	-	X	X	X	SN/GB/AG
30	Glarus	GLA	47 02 / 09 04	723 750 / 210 580	515	-	-	X	-	X	-	X	-	-	X	-	KB/GB
31	Genève-Cointrin	GVE	46 15 / 06 08	498 580 / 122 320	420	X	X	X	X	X	X	X	X	-	X	-	SH/GB/RF/FR
32	Zürich-Kloten	KLO	47 29 / 08 32	682 280 / 259 220	436	X	X	X	X	X	X	X	X	-	X	-	SH
33	Gütsch	GUE	46 39 / 08 37	690 140 / 167 590	2287	X	X	X	X	X	X	X	X	-	-	-	SH/GB
34	Pully	PUY	46 31 / 06 40	540 820 / 151 500	461	-	-	X	-	X	-	X	-	X	X	X	KB/GB/AG
35	Grand-St-Bernard	GSB	45 52 / 07 10	579 200 / 079 720	2472	-	-	X	-	X	-	X	-	-	-	-	KB/GB/RF
36	Adelboden	ABO	46 30 / 07 34	609 400 / 148 975	1320	-	-	X	-	X	-	X	-	X	X	Y	KB/AG/RF
37	Visp	VIS	46 18 / 07 51	631 150 / 128 020	640	-	-	X	-	X	-	X	-	X	X	X	KB/AG
38	La Chaux-de-Fonds	CDF	47 05 / 06 48	551 290 / 215 150	1018	-	-	X	-	X	-	X	-	X	X	Y	SN/GB/AG/RF
39	Rünenberg	RUE	47 26 / 07 53	633 250 / 253 840	610	-	-	-	-	-	-	-	-	X	X	X	KB/AG
40	Buchs-Suhr	BUS	47 23 / 08 05	648 400 / 248 380	387	-	-	X	-	X	-	X	-	X	X	X	KB/GB/AG/RF
41	Luzern	LUZ	47 02 / 08 18	665 520 / 209 860	456	-	-	X	-	X	-	X	-	-	X	-	KB/GB
42	Engelberg	ENG	46 49 / 08 25	674 150 / 186 060	1035	-	-	X	-	X	-	X	-	-	X	-	KB/GB
43	Schaffhausen	SHA	47 41 / 08 37	688 700 / 282 800	437	-	-	X	-	X	-	X	-	-	X	-	KB/GB
44	Zürich-SMA	SMA	47 23 / 08 34	685 125 / 248 090	556	-	-	X	X	X	X	X	-	X	X	X	SH/GB/AG/RF
45	San Bernardino	SBE	46 28 / 09 11	734 120 / 147 270	1639	X	X	X	X	X	X	X	X	-	-	-	SN/GB
46	Weissfluhjoch	WFJ	46 50 / 09 49	780 600 / 189 630	2690	-	-	X	-	X	-	X	-	-	-	-	KB/GB
47	Curvatsch	COV	46 25 / 09 49	783 160 / 143 525	3315	-	-	-	X	-	X	-	-	-	-	-	SN
48	Basel-Binningen	BAS	47 33 / 07 35	610 850 / 265 620	316	-	-	X	-	X	-	X	-	X	X	X	KB/GB/AG/RF
49	Robbia	ROB	46 21 / 10 04	801 850 / 136 180	1078	X	X	X	X	X	X	X	X	X	X	X	SN/AG/
50	Scuol	SCU	46 48 / 10 17	817 130 / 186 400	1300	-	-	X	-	X	-	X	-	-	X	Y	KB/GB/AG
51	Changins	CGI	46 24 / 06 14	507 280 / 139 170	430	-	-	-	-	-	-	-	-	X	X	X	KS/AG/FR
52	La Frêtaz	FRE	46 50 / 06 35	534 230 / 188 080	1202	-	-	-	-	-	-	-	-	X	X	-	KS/AG
53	Bern-Liebefeld	BER	46 56 / 07 25	598 610 / 197 470	565	-	-	X	-	X	-	X	-	X	X	X	KB/GB/AG
54	Güttingen	GUT	47 36 / 09 17	738 430 / 273 950	440	-	-	X	-	X	-	X	-	X	X	-	KB/GB/AG/RF
55	Gösgen	GOE	47 22 / 07 59	641 260 / 246 130	380	-	-	-	-	-	-	-	-	-	-	-	KKW
56	Wädenswil	WAE	47 13 / 08 41	693 770 / 230 780	463	-	-	-	-	-	-	-	-	X	X	X	KS/GB/AG/FR
57	Tänikon	TAE	47 29 / 08 54	710 500 / 259 820	536	-	-	X	-	X	-	X	-	X	X	X	KB/AG
58	Reckenholz	REH	47 26 / 08 31	681 400 / 253 550	443	-	-	-	-	-	-	-	-	X	X	X	KS/AG
59	Locarno-Monti	OTL	46 10 / 08 47	704 160 / 114 350	366	-	-	X	X	X	X	X	-	X	X	-	SH/GB/AG
60	Beznau	BEZ	47 34 / 08 14	659 500 / 267 400	327	-	-	-	-	-	-	-	-	-	-	-	KKW
61	Mühleberg	MUB	46 59 / 07 17	587 850 / 202 450	483	-	-	-	-	-	-	-	-	-	-	-	KKW
62	Cimetta	CIM	46 12 / 08 48	704 370 / 117 515	1672	-	-	-	-	-	-	-	-	-	-	-	KS
63	Evolène-Villa	EVO	46 07 / 07 31	605 415 / 106 740	1825	-	-	X	-	X	-	X	-	-	-	-	GB
64	Leibstadt	LEI	47 36 / 08 11	656 350 / 272 100	341	-	-	-	-	-	-	-	-	-	-	-	KKW
65	Fey	FEY	46 11 / 07 16	586 725 / 115 180	737	-	-	-	-	-	-	-	-	-	-	-	GB
66	Grimsel-Hospiz	GRH	46 34 / 08 20	668 460 / 158 160	1980	-	-	X	-	X	-	X	-	-	-	-	KB/RF
67	Comprovasco	COM	46 28 / 08 56	714 998 / 146 440	575	-	-	-	-	-	-	-	-	X	X	X	KB/AG/RF
68	Lägern	LAE	47 29 / 08 24	672 250 / 259 460	868	-	-	-	-	-	-	-	-	-	-	-	GB
69	Hörnli	HOE	47 22 / 08 57	713 500 / 247 750	1144	-	-	-	-	-	-	-	-	-	-	-	KS
70	Plaffeien	PLF	46 45 / 07 16	586 850 / 177 400	1042	-	-	X	-	X	-	X	-	-	X	-	GB
71	Robiei	ROE	46 27 / 08 31	682 600 / 144 075	1898	-	-	-	-	-	-	-	-	-	-	-	GB
72	PSI Würenlingen	PSI	47 32 / 08 14	659 540 / 265 600	334	-	-	-	-	-	-	-	-	-	-	-	KKW

Key:

Type of station::

SH	principal synoptic station
SN	additional synoptic station
KB	weather report station
KS	weather station (no visual observation)
KKW	station based at a nuclear plant (mast)
RF	reference station
GB	Green Bulletin station
AG	station taking agrometeorological measurements
FR	station taking frost measurements
RA	radiosondes station
X	from 1 April to 1 October
Y	from 1 June to 1 October

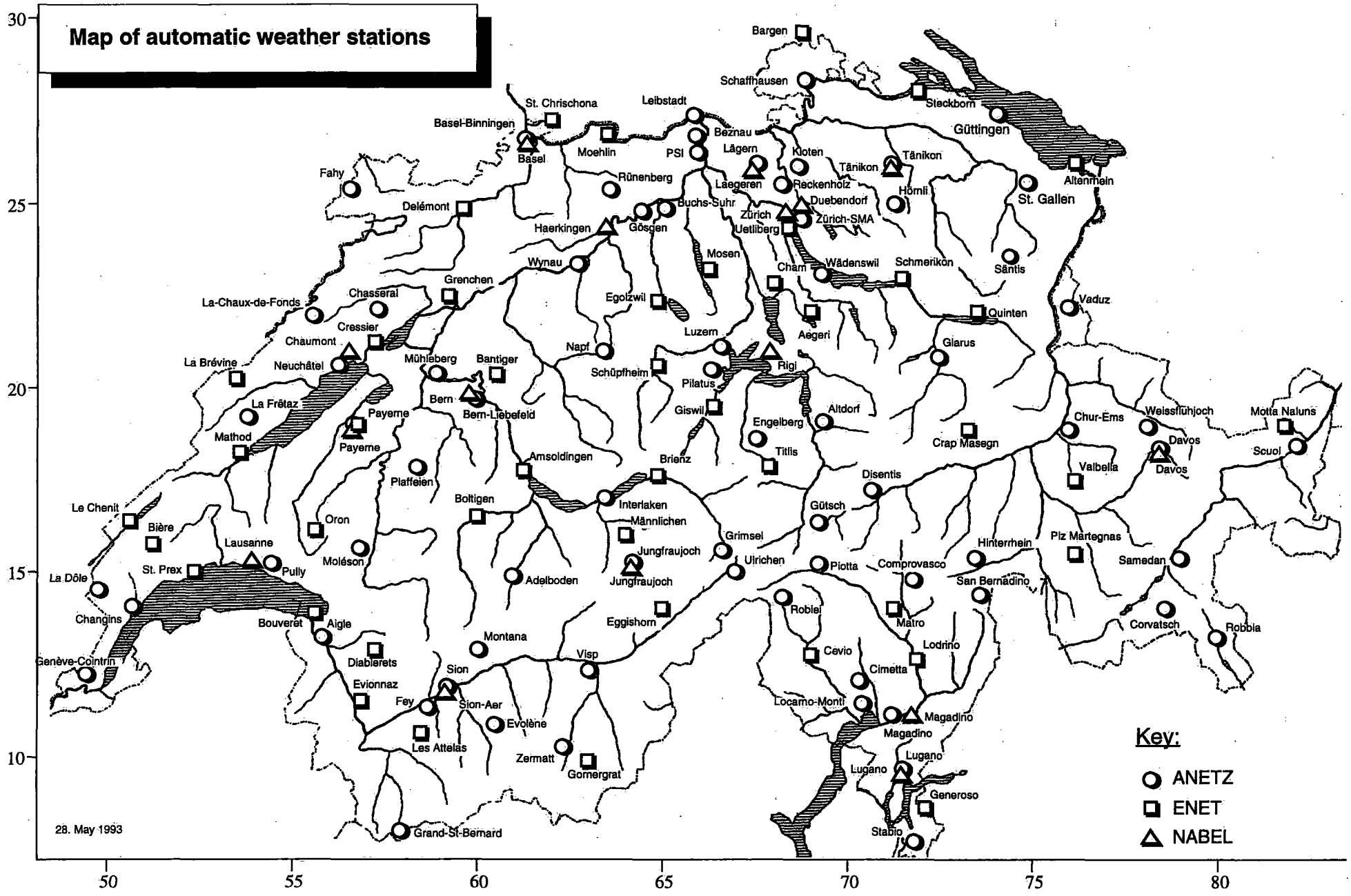
Map of automatic weather stations
Bargen
Schaffhausen
Steckborn
Güttingen
St. Chrischona
Leibstadt
Basel-Binningen
Basel
Moehlin
PSI
Beznau
Lägern
Kloten
Tänikon
Tänikon
Altenrhein
St. Gallen
Fahy
Rünenberg
Laegeren
Reckenholz
Hörnli
Delémont
Buchs-Suhr
Duebendorf
Zürich
Zürich-SMA
Uetliberg
Haerkingen
Gösgen
Mosen
Wynau
Cham
Wädenswil
Schmerikon
Säntis
Grenchen
Egolzwil
Vaduz
La-Chaux-de-Fonds
Chasseral
Quinten
Cressier
Luzern
Aegeri
Napf
Glarus
Chaumont
La Brévine
Neuchâtel
Mühleberg
Bantiger
Schüpfheim
Pilatus
Rigi
Bern
Bern-Liebefeld
La Frêtaz
Giswil
Altdorf
Engelberg
Chur-Ems
Weissfluhjoch
Motta Naluns
Payerne
Payerne
Mathod
Titlis
Crap Masegn
Davos
Davos
Scuol
Amsoldingen
Brienz
Valbella
Plaffeien
Disentis
Le Chenit
Boltigen
Interlaken
Gütsch
Oron
Bière
Männlichen
Grimsel
Hinterrhein
Plz Martegnas
Lausanne
Jungfraujoch
Moléson
Ulrichen
Piotta
Comprovasco
Samedan
St. Prex
Pully
Jungfraujoch
San Bernadino
La Dôle
Adelboden
Robiei
Changins
Bouveret
Aigle
Eggishorn
Matro
Corvatsch
Robbia
Montana
Lodrino
Genève-Cointrin
Diablerets
Visp
Cevio
Sion
Cimetta
Evionnaz
Fey
Sion-Aer
Locarno-Monti
Magadino
Evolène
Magadino
Les Attelas
Lugano
Zermatt
Gornergrat
Lugano
Generoso
Stabio
Grand-St-Bernard
28. May 1993
Key:
ANETZ
ENET
NABEL
30
25
20
15
10
50
55
60
65
70
75
80